OUKA
The University of Osaka
Institutional Knowledge Archive

Title	Microbomb Combustion Calorimetry of Non-planar Aromatic Hydrocarbons
Author(s)	清林, 哲
Citation	大阪大学, 1995, 博士論文
Version Type	VoR
URL	https://doi.org/10.11501/3108019
rights	
Note	

The University of Osaka Institutional Knowledge Archive : OUKA

https://ir.library.osaka-u.ac.jp/

The University of Osaka

DOCTORAL THESIS

Microbomb Combustion Calorimetry of Non-planar Aromatic Hydrocarbons

by
Tetsu Kiyobayashi

Microcalorimetry Research Center
Faculty of Science
Osaka University

1995

Contents

1 General Introduction 11
- 1.1 Intrduction . . . 11
- 1.2 State of the Art of Microcombustion Calorimetry . . . 12
- 1.3 Motif of the Present Study . . . 13

2 Micro-bomb Combustion Calorimetry 15
- 2.1 Introduction . . . 15
- 2.2 Description of the apparatus . . . 16
  - 2.2.1 Micro-bomb . . . 16
  - 2.2.2 Calorimeter . . . 16
- 2.3 Measurement and calculation . . . 19
  - 2.3.1 Measurement System . . . 19
  - 2.3.2 Combustion experiment . . . 21
  - 2.3.3 Calibration experiments . . . 21
  - 2.3.4 Calibration of the electric energy . . . 22
  - 2.3.5 Calculation . . . 23
- 2.4 Testing of the calorimeter . . . 25
- 2.5 Performance of the new calorimeter . . . 25

3 Combustion Calorimetry of C_{60} and C_{70} 37
- 3.1 Introduction . . . 37
- 3.2 Experimental . . . 37
- 3.3 Results and Discussion . . . 41

4 Combustion Calorimetry of Corannulene 45
- 4.1 Introduction . . . 45
- 4.2 Experimental . . . 45
- 4.3 Result . . . 48
- 4.4 Experimental and Theoretical $\Delta_f H°$ . . . 50

5 Combustion Calorimetry of Coronene 53
- 5.1 Introduction . . . 53
- 5.2 Experimental . . . 54
- 5.3 Result and Discussion . . . 60

6 Energetics of PBAH **63**
6.1 Introduction 63
6.2 Resonance Energy of PBAH 64
6.3 Additivity Scheme with Resonance Energy 65
6.4 Evaluation and Discussion 67

7 Energetics of Carbon Clusters **71**
7.1 Introduction 71
7.2 Haddon's POAV Analysis 72
7.3 Strain and Resonance Energies of Fullerene 73
7.3.1 Curvature and Strain of Fullerene 73
7.3.2 Resonance Energy Diminution 74
7.3.3 Evaluation and Discussion 75
7.4 Fullerene, Onion and Graphite 80

8 Concluding Remarks **87**

List of Figures

2.1 Micro-bomb 17
2.2 Isoperibol Combustion Calorimeter 18
2.3 Calorimetric System 20
2.4 Scatter of the temperature data from smoothed curves 29
2.5 Electric potential, current, resistance and power for microheater 31
2.6 Electric potential, current, resistance and power for ignition 32
2.7 Resistance of microheater during combustion – how microheater works . . 33
2.8 Resistance of microheater during combustion – sample dependency 34
2.9 Calculated adiabatic temperature rise as a function of reaction period . . . 35

3.1 C_{60} and C_{70} 38
3.2 Mass spectra of C_{60} and C_{70} 39

4.1 Corannulene $C_{20}H_{10}$ 46

5.1 Coronene $C_{24}H_{12}$ 54
5.2 ^{1}H-NMR signals of the crude coronene sample. 55
5.3 Liquid chromatogram of coronene 56
5.4 Candidates of impurities in coronene 57

7.1 Cyvin's in-plane force constants 76
7.2 Molecular structure of corannulene 77
7.3 Pyracylene (Cyclopent[*fg*]acenaphthylene) 78
7.4 η^2- and η^5-Complexes 78
7.5 Formation enthalpies of fillerenes, onions and graphite fragments 86

List of Tables

0.1 Standard formation and atomization enthalpies of C_{60}, C_{70}, corannulene and coronene 7

1.1 World's microbomb combustion calorimeters 12

2.1 Auxiliary data for benzoic acid and salicylic acid 23
2.2 Results of calibration for salicylic acid with benzoic acid 26
2.3 Results of calibration for salicylic acid with the internal microheater 27
2.4 Corrected energy equivalents 27
2.5 Results of combustion of salicylic acid 28
2.6 Standard thermodynamic quantities of salicylic acid 30

3.1 Results of calibration for C_{60} and C_{70} 40
3.2 Results of combustion calorimetry of C_{60} and C_{70} 42
3.3 Standard thermodynamic quantities 43
3.4 Comparison with reported values 43

4.1 Results of calibration for corannulene 47
4.2 Results of combustion of corannulene 49
4.3 Standard thermodynamic quantities 50
4.4 Comparison among experiments and theoretical calculations 51

5.1 Results of calibration for coronene 58
5.2 Results of combustion calorimetry of coronene 59
5.3 Sublimation enthalpies of coronene 60
5.4 Standard thermodynamic quantities of coronene 61
5.5 $\Delta_f H^\circ$(g) of coronene: experimental and calculated values 62

6.1 Experimental $\Delta_f H^\circ$, $\Delta_a H^\circ$, and TRE for PBAHs 65
6.2 Experimental and predicted $\Delta_a H^\circ$ for PBAHs 68
6.3 Contributions of resonance energy to the atomization enthalpy and predicted formation enthalpies 69

7.1 Resonance and strain energies, etc of corannulene ($C_{20}H_{10}$), C_{60} and C_{70} . 75
7.2 Formation enthalpies of hollow fullerenes and fullerene onions 85

Abstract

A micro-bomb combustion calorimeter was developed. The formation and atomization enthalpies of C_{60}, C_{70}, corannulene and coronene were determined by this calorimeter. Derived results are summarized in Table 0.1. Comparison of these formation enthalpies

Table 0.1: Standard formation and atomization enthalpies of C_{60}, C_{70}, corannulene and coronene at 298.15K in kJ·mol^{-1}

	$\Delta_f H°$(c)	$\Delta_f H°$(g)	$\Delta_a H°$(g)
C_{60}	2273±15	2501±17	40498±31
C_{70}	2369±18	2536±20	47531±37
Corannulene	342.3±5.6	463.7	16050
Coronene	152.5±6.9	295.4±9.1	19521±14

with those of several theoretical calculations suggests the rectification of parameters is necessary for semi-empirical methods to predict the formation enthalpies of non-planar molecules.

Experimental atomization enthalpies of seven planar polycyclic benzenoid aromatic hydrocarbons (PBAHs), benzene, naphthalene, anthracene, pyrene, naphthacene, coronene and graphite were fitted to the three-parameter function of the form:

$$\Delta_a H° = n_{CC}E_{CC} + n_{CH}E_{CH} + TRE\beta$$

where n_{CC} and n_{CH} are respectively numbers of CC and CH bonds, E_{CC} and E_{CH} are bond energies of hypothetical localized CC and CH bonds, respectively, TRE is the topological resonance energy, and β is the Hückel resonance integral. Despite only three adjustable parameters in the equation, atomization enthalpies of these planar PBAHs were well reproduced with the parameters E_{CC}/kJ·mol^{-1} = 462.6, E_{CH}/kJ·mol^{-1} = 441.6 and β/kJ·mol^{-1} = 362.2.

Parameters determined above were used to evaluate the strain energies of C_{60}, C_{70} and corannulene from the experimental atomization enthalpies. A competing relation between resonance energy and strain energy in these non-planar molecules was derived quantitatively. The strain energies of C_{60}, C_{70} and corannulene are 1707, 1754 and 195.7 in kJ·mol^{-1}, respectively. The fact that the strain energies of C_{60} and C_{70} are similar to each other supports the "curvature conservation law of fullerenes". By virtue of the separation of atomization enthalpy into resonance energy and localized bond energy, the strain of non-planar molecule was found to be explained by a simple force-constant model. The relative stabilities among single-shelled fullerenes, multi-shelled fullerenes (fullerene onions) and graphite fragments were predicted in terms of the parameters determined in the present study. For a collection of about a thousand carbon atoms the most stable form is predicted to be the fullerene onions.

要　旨

微量燃焼熱量計を開発し、それを以て C_{60}、C_{70}、コラヌレン、コロネンの標準生成エンタルピー及び原子化エンタルピーを決定した。得られた結果を表 0.1 に掲げる。実験で得られた標準生成エンタルピーを幾つかの理論計算値と比較してみたところ、半経験的手法は非平面分子の標準生成エンタルピーを正しく予測するためには何らかの改良が不可欠であることが示された。

七つの平面型多環ベンゼノイド芳香族炭化水素 (PBAH)、ベンゼン、ナフタレン、アントラセン、ピレン、コロネン、及びグラファイトに対する原子化エンタルピーの実験値を以下の３パラメータ関数に最適化した。

$$\Delta_a H^\circ = n_{CC}E_{CC} + n_{CH}E_{CH} + TRE\beta$$

ここで n_{CC}、n_{CH} は各々 CC結合、CH結合の数であり、E_{CC}、E_{CH} は各々局在した仮想的 CC結合、CH結合のエネルギー、TRE は位相幾何共鳴エネルギー、β はヒュッケル共鳴積分である。この関数は僅か３パラメータであるにも関わらず、E_{CC}/kJ·mol^{-1}= 462.6,

$E_{CH}/kJ{\cdot}mol^{-1} = 441.6$ and $\beta/kJ{\cdot}mol^{-1} = 362.2$ を以てこれら平面型 PBAH の原子化エンタルピーをよく再現した。

上で得られたパラメータの値を実験で得られた原子化エンタルピーから C_{60}、C_{70} 及びコラヌレンの歪エネルギーを算出するのに用い、これら非平面分子における共鳴エネルギーと歪エネルギーの競合関係を定量的に評価した。C_{60}、C_{70} 及びコラヌレンの歪エネルギーは各々 1707、1754、195.7 $kJ{\cdot}mol^{-1}$ と計算された。C_{60}とC_{70}の歪エネルギーが近いことからフラーレンにおける「曲率保存則」が確認された。原子化エンタルピーを共鳴エネルギーと局在結合エネルギーに分離したことにより非平面分子の歪エネルギーが簡単な力場モデルで説明されることが分かった。単殻フラーレン、多殻フラーレン（フラーレンオニオン）、グラファイト片の相対的安定性の予測を行い、1000 炭素原子程度の集合では多殻フラーレンが最安定であることを明らかにした。

Chapter 1

General Introduction

1.1 Intrduction

The formation enthalpy (and atomization enthalpy) of a compound is one of thermodynamic quantities which plays the central role in thermochemistry. From the compilation of formation enthalpies, one can evaluate the reaction enthalpies and relative stabilities among many substances. In applied chemistry, these values provide a quantitative measure in the search for rational and effective synthetic procedures. From the theoretical point of view, these values are of fundamental importance for the energetics of intramolecular bonds, the structure-energy relationship, and so on.

In 1784, year of which is before the proposal of the first law of thermodynamics, Lavoisier and de Laplace first mentioned the combustion calorimetry in *"Mémoire sur la chaleur (Memoir on the heat)"* [1] (For comprehensive history of combustion calorimetry, see Chapter 18 of ref. [2]). The most sophisticated technique for the determination of formation enthalpy of organic compounds is still today the combustion calorimetry. Recent development of synthetic techniques in organic chemistry has made a large number of interesting molecules available for such a study, though often in a small amount and/or at a high cost. Since combustion calorimetry is a very destructive method, the miniaturization of the calorimeter has been thus an urgent necessity.

1.2 State of the Art of Microcombustion Calorimetry

Table 1.1: World's microbomb combustion calorimeters

	A:Lund[a]	B:Lisboa[b]	C:Freiburg[c]
Type	isoperibol stirred water	isoperibol stirred gas (He)	isoperibol aneroid (Cu)
Bomb rotaion	No	Yes[k]	No
Thermometer	thermistor	thermistor	quartz
V_{bomb}[g]/cm^3	4.5	18	45
m_B[h]/mg	10	20-40	50
ϵ°[i]/J·K^{-1}	583	1810	1481
s.d.m.[j]/%	0.020	0.016	0.018

	D:Marseille[d]	E:Osaka[e]	F:Osaka[f]
Type	heat flow twin	isoperibol stirred water	isoperibol stirred water
Bomb rotaion	Yes	No	Yes
Thermometer	thermopile	thermistor	thermistor
V_{bomb}[g]/cm^3	43	9	347
m_B[h]/mg	5	20	1040
ϵ°[i]/J·K^{-1}	15.96[l]	1375	15350
s.d.m.[j]/%	0.040	0.020	0.003

[a]University of Lund. Månsson *et al.* [12]. [b]Instituto Superior Técnico. Minas da Piedade *et al.* [17]. [c]Universität Freiburg. Beckhaus *et al.* [16]. [d]Centre de Thermodynamique et de Microcalorimétrie. Sabbah *et al.* [15]. [e]The present calorimeter. Microcalorimetry Research Center. See Chapter 2. [f]Microcalorimetry Research Center. Macro combustion calorimeter. Sakiyama *et al.* [18]. [g]Inner volume of combustion bomb. [h]Mass of benzoic acid for calibration of the calorimeter. [i]Energy equivalent of the standard calorimetric system. [j]Standard deviation of the mean of ϵ°. [k]Under test. [l]Unit is in J·V^{-1}·s^{-1}.

The reduction of the amount of sample neccessary for one combustion experiment to about or less than one hundred milligram was first attempted in the 1920's at several laboratories [5, 6, 7]. After the Second World War, more sophisticated miniature combustion calorimeters appeared [8, 9, 10, 11], though all of them are now no longer in operation. An overview of the current activity of miniature combustion calorimetry is shown in Table 1.1.

For comparison, a macro combustion calorimeter F is shown in the table. The calorimeter B was originally constructed at University of Lund as a joint project with Manchester University. The calorimeter D is of heat-flow type, while the others are isoperibol. In order to reduce the temperature inhomogeneity in the calorimeter, stirred water is used in the calorimeters A, E and F. In the calorimeter B and C, the heat-transmitting media are stirred helium gas and copper block, respectively. Bomb rotation is necessary to realize a well-defined final state for combustion calorimetry of organic sulfur or halogenated compounds (B, D and F). Intrinsic difficulties in miniaturizing the calorimeter and how we could get over them are described in the next chapter.

1.3 Motif of the Present Study

The discovery of the fullerene as a third allotrope of carbon has revitalized the fundamental concepts of physical chemistry. There are two major subjects that intrigue us:

- What are the roles of aromaticity and strain in a fullerene molecule and how they relate with each other?
- Why the significant amount of fullerene is produced in the harsh environment (e.g. arc-discharge between carbon electrodes) in spite of the fact that the most stable state of carbon is graphite at the ambient temperature and pressure?

The aim of the present study should be thus orientated towards how to shed light on these issues. As described in Chapter 6 and Chapter 7, several theoretical concepts have been proposed to figure out the physical and chemical nature of the fullerenes. Some of them emphasize the aromatic character and the others do the strain of curved surface. However, unified quantitative description of aromaticity and strain in a fullerene molecule has not been attained so far.

In the present study, an empirical treatment on the energetics for curved sp^2-carbon clusters is proposed in terms of the resonance energy and strain energy, i.e., concrete values of energy are attributed to the terms "resonance" and "strain" by using solely experimental thermochemical data and structural information. As an initial step of setting

up the energetics, strain-free conjugate molecules are considered in Chapter 6 utilizing the experimental results of Chapter 5, and the unit of the resonance energy is evaluated. Then in Chapter 7, the strain energy is introduced and its unit is evaluated from the results of Chapters 3 and 4.

A simple force-constant model is proposed in order to explain the origin of the strain energy in non-planar molecule. Finally, the relative stabilities are discussed of hollow fullerenes, fullerene onions and graphite fragments of given number of carbon atoms.

Chapter 2

Micro-bomb Combustion Calorimetry *

2.1 Introduction

In our laboratory, a microbomb calorimeter was developed several years ago [19]. Through the use of this calorimeter, various difficulties have been experienced. In the present study, a new microbomb combustion calorimeter was used that incorporated improvements removing previously experienced difficulties.

Several difficulties have to be overcome in the miniaturization of a bomb combustion calorimeter while retaining the accuracy and precision achieved in macrobomb combustion calorimetry. Difficulties related to the reduction of the mass of the sample and the energy to be measured are common to every sort of microcalorimetry including combustion, vapourization, reaction and heat capacity calorimetries. A difficulty inherent in combustion calorimetry is the achievment of complete combustion of the sample. Owing to the increase of the surface area relative to the mass of a sample, the heat transfer from a burning sample becomes more effective with decrease of the mass. Consequently, the temperature of a burning sample is decreased below the lowest value required for the combustion to be sustained to the completion. Hence, special attention must be paid for the achievment of complete combustion. Otherwise incomplete combustion is encountered.

Generally speaking, organic compounds with a large C/H ratio are prone to incomplete combustion. Since these are exactly the type of molecules to be studied in the present study, a new micro-bomb combustion calorimeter was developed that allowed the sample

*The main part of this chapter will be submitted to *J. Chem. Thermodyn.* under the names of Sakiyama, M.; Kiyobayashi, T.

to be kept at a high enough temperature all through the combustion reaction. In this calorimeter, the lowering of temperature of a burning sample in the final stage of combustion can be delayed by supplying electric power to a microheater installed under the combustion crucible.

2.2 Description of the apparatus

2.2.1 Micro-bomb

The cross-sectional view of the micro-combustion bomb is shown in Figure 2.1. The main part of the bomb (internal volume is about 9 cm^3) is made of stainless steel. The upper part of the the bomb is double-walled and the inner surface of the inner wall (1 mm thickness) is covered with platinum plate A. The outer surface of the top of the internal wall is coated with alumina cement B and the space enclosed by the two walls is filled with granular zirconia insulater C. The bomb is equipped with a micro-valve D and two independent insulated electrodes E; one for ignition of the sample and the other for power supply to an internal microheater described below. The valve is horizontally arranged under the main body and has no connections with the line for charging and discharging of the gas, so that the total length of the bomb is minimized. High pressure oxygen is charged, after fixing the bomb to a rigid metal frame, through a small hole under the valve and a rubber "O" ring of a gas charge-discharge line attached to the metal frame.

An important innovation in the design of the present microbomb is the installation of an internal microheater F under a platinum crucible G for the achievement of complete combustion of the sample. The microheater is made with a bifilarly and circularly wound piece of platinum wire (0.1 mm in diameter) and adhered to the outer surface of the bottom of the crucible with alumina cement, the total resistance being about 2.5 Ω. The total of the crucible and the microheater is supported by a thin alumina pipe H of 1 mm in outer diameter.

2.2.2 Calorimeter

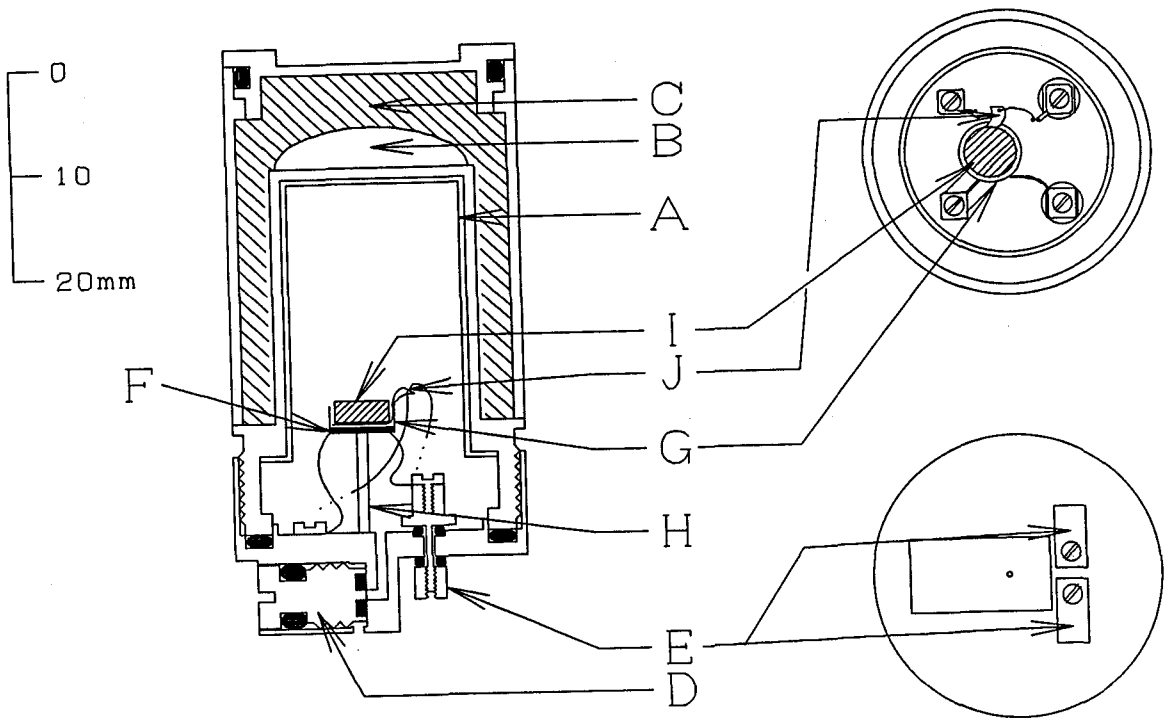

A: Platinum liner. B: Alumina cement. C: Granular zirconia insulator.
D: Micro-valve. E: Electrodes. F: Micro-heater. G: Platinum crucible.
H: Alumina strut. I: Sample pellet. J: Polyethylene fuse.

Figure 2.1: Micro-bomb

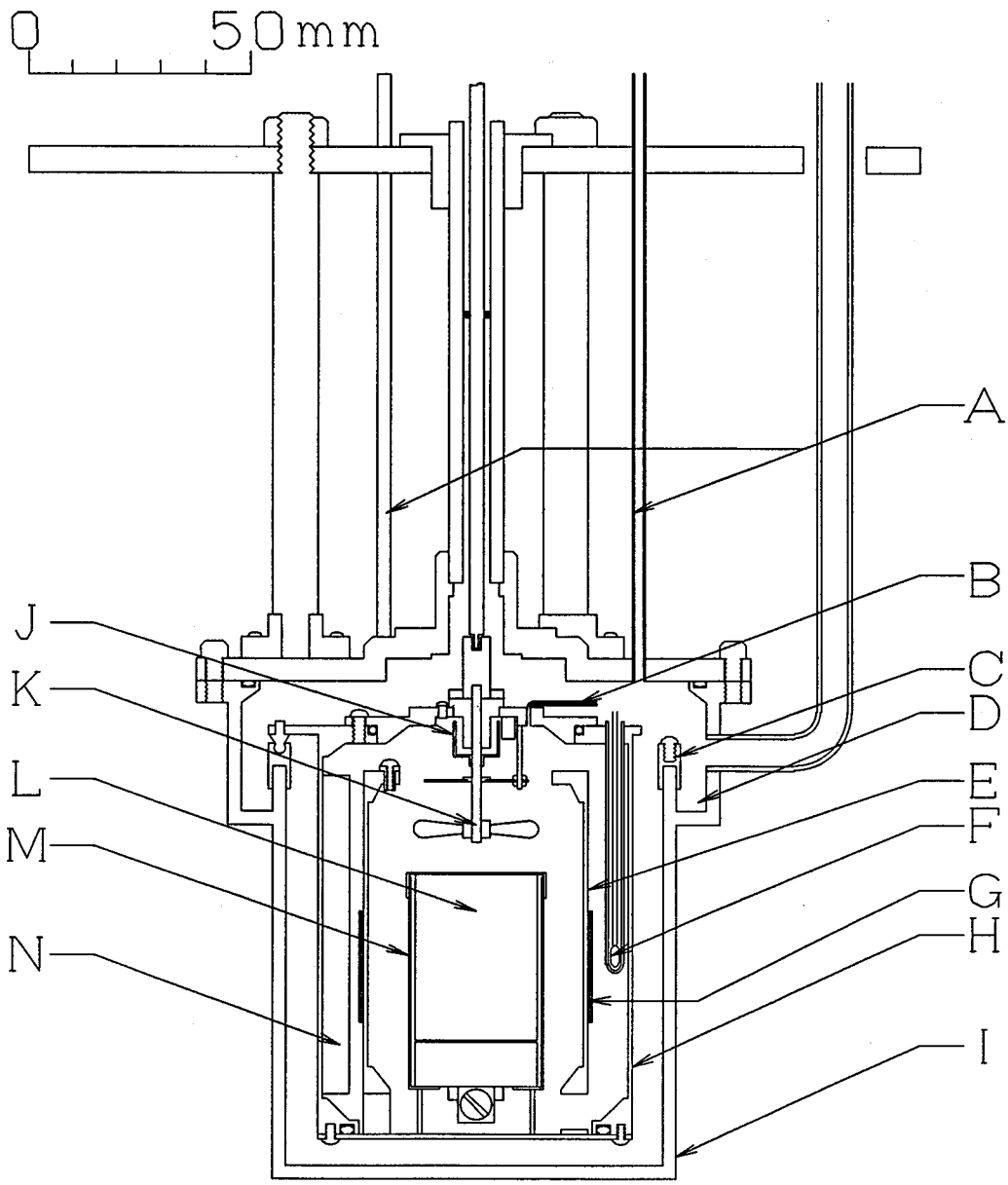

A: Ventilation tubes. B: capillary tube. C: Terminals. D: Circular groove. E: Partition wall. F: Thermistor. G: Pre-heater. H: Calorimeter proper. I: Isoperibol vessel. J: Oil seal. K: Stirrer. L: Micro-bomb. M: Copper can. N: Radial vanes.

Figure 2.2: Isoperibol Combustion Calorimeter

The cross-sectional view of the calorimeter is shown in Figure 2.2. The calorimeter is a stirred-liquid type isoperibol calorimeter with flow pattern control. The calorimeter proper H sits in a submarine vessel I with an air gap of about 7 mm between two walls and positioned on the V-shaped hollow of Delrin supports with three balls. The air gap is ventilated by blowing in a stream of air through the ventilation tubes A before the temperature acquisition started. The submarine vessel is immersed in a commercial water thermostat (Tronac Precision Temperature Controller PTC 40 and Komatsu Coolnics Circulator CTE220/CTR220). Temperature of the thermostat is regulated within 0.3 mK at about 298.4 K. For the purpose of flow pattern control, a partition wall E and eight symmetrically disposed copper radial vanes N are installed. The bomb L is encased in a copper can M for the same purpose. A Nichrome V heater wire G for the preheating of the calorimetric water is wound bifilarly around the partition wall. The brass calorimeter can H is sealed with rubber "O"-rings and an oil seal J and filled with a constant mass of water to a level leaving a small air space communicating to the space above the thermostat water through capillary tube B. The temperature of calorimetric water is measured with a thermistor F with the resistance of about 10 kΩ at 273 K. Lead wires are introduced into the calorimeter proper through a bent side tube of the calorimeter vessel, tempered with thermostat temperature in the circular groove D by using Wood's metal and finally connected to circularly disposed terminals C. The stirrer rod K is connected with a motor-driven metal shaft via a plastic insulator.

2.3 Measurement and calculation

2.3.1 Measurement System

The block diagram of the present calorimetric system is shown in Figure 2.3. The measurement is fully automated by using a personal computer.

The resistance of the thermistor, which detects the temperatures of the calorimeter water, forms an arm of a Wheatstone bridge fixed at an appropriate dial setting. The off-balance signal was measured with a nanovoltmeter (Keithley 181) down to the digit of 10 nV. A mean of about 800 acquired data is stored in a RAM of the personal computer at every

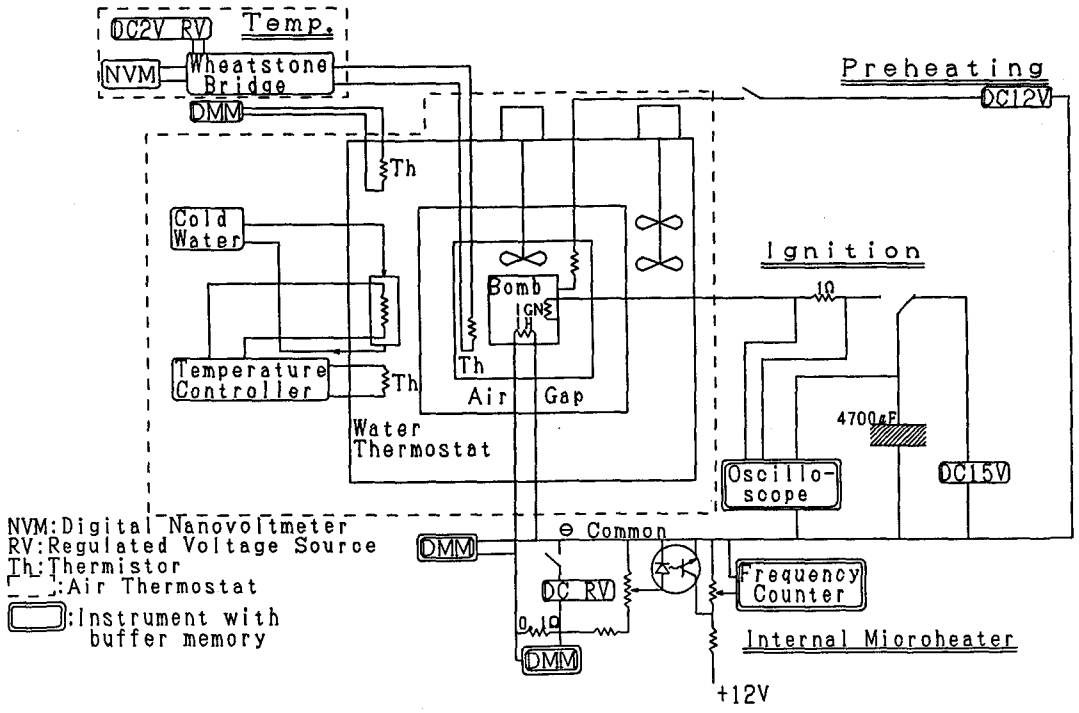

Figure 2.3: Calorimetric System

10 s interval. The temperature measurement system is placed in an air thermostat.

The potential difference across the microheater (and lead wires connected to it in the calorimeter proper) is measured at the terminals on the submarine vessel with a digital multimeter (Keithley 199) and the corresponding current is measured from the potential difference across a 0.1 Ω standard resistor with a digital multimeter (Keithley 196). The digital voltmeters have a buffer memory of 500 data each. They are triggered simultaneouly and data are acquired at an identical interval and stored in each buffer memory. After an experiment, the both potential difference data acquired are fed to a RAM of the personal computer and electric power is calculated from the data acquired. Heating time is measured by triggering a universal frequency counter (Hioki 3601), operating in the time interval mode, by the heating current of the microheater via a photocoupler.

The sample is ignited by the discharge of a 4700 μF capacitor charged up to 15 V. A two-channel storage oscilloscope (Tektronix 2221) was used to determine the electric power for ignition. The method of measurement is similar to that for the power for the microheater.

2.3.2 Combustion experiment

The experiment is composed of initial, reaction, and final periods, each with a length of 1800 s. In each period, 180 data of the calorimeter temperatures are collected. At 1810 s from the start of data acquisition, the sample is ignited and at 1811 s the power supply to the microheater is started. The length of heating time is variable, a standard length being 19 s. Because of the buffer memories possessed by the electronic apparatus for measurement, only the starter signals for ignition and for energizing the microheater are dispatched to an interface via a parallel input and output (PIO) circuit of the personal computer. The computer is otherwise devoted to acquisition of the temperature data.

2.3.3 Calibration experiments

The calorimeter proper is calibrated by burning the thermochemical standard benzoic acid (NIST SRM 39i). Since the electric energy is supplied to the microheater in a combustion experiment, the supplied electric energy is also calibrated against the standard benzoic

acid. For this purpose, a set of two measurements by different modes are carried out; one is the calibration experiment by benzoic acid combustion with supply of a small amount of electric energy through the microheater, which is similar to a sample combustion experiment described below, the other following the first, after cooling the submarine vessel without changing its arrangement, is an *in situ* calibration experiment using only electric energy supplied to the microheater. In the calibration experiment by the second mode, the supplied power to the microheater is similar to that for a sample or benzoic acid combustion experiment while the total energy has to be equal to that of the actual combustion experiment. Accordingly the period of heating is extended to 160 s, the period of data acquisition being 320 ms (38 ms for a sample combustion or benzoic acid combustion experiment in the case of heating period of 19 s).

2.3.4 Calibration of the electric energy

The correction factor to be multiplied with the observed (nominal) electric energy E_{el} supplied to the microheater to obtain the heat Q actually evolved from the microheater into the calorimeter is denoted as f, i.e.

$$f = \frac{Q}{E_{\mathrm{el}}}. \tag{2.1}$$

In the case of a calibration experiment by the first mode, the energy equivalent of an empty calorimetric system ϵ° is expressed as follows:

$$\epsilon^{\circ} = \frac{-\Delta_{\mathrm{IBP}} U + \epsilon^{\mathrm{i}} (T_{\mathrm{i}} - T_{\mathrm{r}}) + \epsilon^{\mathrm{f}} (T_{\mathrm{r}} - T_{\mathrm{f}} + \Delta T_{\mathrm{c}}) + f \cdot E_{\mathrm{el}} + E_{\mathrm{ign}}}{\Delta T_{\mathrm{ad}}} \tag{2.2}$$

where $\Delta_{\mathrm{IBP}} U$ is the internal energy change for the isothermal bomb process, T_{i} and T_{f} are respectively the initial and final temperatures of the reaction period, ΔT_{c} is the correction term for heat exchange with the surroundings and for the inernal heat evolution during the reaction period (due to stirring of calorimeter water and Joule heating of the thermistor), ΔT_{ad} ($\equiv T_{\mathrm{f}} - T_{\mathrm{i}} + \Delta T_{\mathrm{c}}$) is the adiabatic temperature rise, ϵ^{i} and ϵ^{f} are the contributions from the contents of the bomb before and after combustion, respectively, to the total energy equivalent, and E_{ign} is the observed ignition energy.

In the case of a calibration experiment by the second mode, the energy equivalent of the empty calorimetric system ϵ° is expressed as follows:

$$\epsilon^\circ = \frac{f \cdot E'_{\mathrm{el}}}{\Delta T'_{\mathrm{ad}}} - \epsilon^{\mathrm{f}} \tag{2.3}$$

where E'_{el} is the observed electric energy supplied to the microheater and $\Delta T'_{\mathrm{ad}}$ is the adiabatic temperature rise for this mode of calibration. From the equations (2.2) and (2.3), the correction factor f is derived by the equation:

$$f = \frac{X}{Y} \tag{2.4}$$

where

$$X = \frac{-\Delta_{\mathrm{IBP}} U + \epsilon^{\mathrm{i}} (T_{\mathrm{i}} - T_{\mathrm{r}}) + \epsilon^{\mathrm{f}} (T_{\mathrm{r}} - T_{\mathrm{f}} + \Delta T_{\mathrm{c}}) + E_{\mathrm{ign}}}{\Delta T_{\mathrm{ad}}} + \epsilon^{\mathrm{f}}$$

and

$$Y = \frac{E'_{\mathrm{el}}}{\Delta T'_{\mathrm{ad}}} - \frac{E_{\mathrm{el}}}{\Delta T_{\mathrm{ad}}}.$$

2.3.5 Calculation

Table 2.1: Auxiliary data for benzoic acid and salicylic acid

Compound	ρ/g·cm^{-3}	c_p/J·K^{-1}g^{-1}	$-\left(\frac{\partial u}{\partial p}\right)_T$ /J·atm^{-1}·g^{-1}
benzoic acid	1.32[a]	1.21[a]	0.012[a]
salicylic acid	1.17[b]	1.44[a]	0.012[c]

[a]Ref. [21]. [b]Ref. [20]. [c]Estimated.

The adiabatic temperature rise is determined as reported previously [18a]. The energy equivalent of the present calorimeter is based on the standard specific energy of combustion of standard benzoic acid, 26413.6 J·g^{-1} at 298.15 K which was derived from the relation:

$$\left|\frac{\Delta_{\mathrm{c}} U_{\mathrm{cert}}}{M}\right| - \left|\frac{\Delta_{\mathrm{c}} U^\circ}{M}\right| = 20.4 \text{ J·g}^{-1}. \tag{2.5}$$

The Washburn's correction was calculated by the reported method [3] and both ϵ^{i} and ϵ^{f} were determined. Auxiliary data for the buoyancy correction and for the reduction to

thermodynamic standard states are given in Table 2.1. The amount of nitric acid, which is formed by oxidation of nitrogen impurity contained in the oxygen gas, was determined by measuring the absorbance of the 202 nm band due to NO_3^- ion.

The correction factor f was calculated by equation (2.4) and used to calculate the energy equivalent of empty calorimeter ϵ°.

2.4 Testing of the calorimeter

The calorimeter was tested by using salicylic acid in the crystalline state as a test material. Salicylic acid (Wako Pure Chemical Industries, Ltd.) was recrystallized four times from distilled water, ground to powder in an agate mortar, and sublimed *in vacuo* at 80 ℃.

In this series, seven sets of calibration experiments were carried out. Derived values of the correction factor f to observed electric energy are 1.00016, 1.00019, 0.99957, 1.00010, 1.00100, 1.00005, and 1.00016 in the order of the experiment number. The mean and standard deviation of the mean is (1.00020 ± 0.00023).

Results of the calibration experiment by the first and second modes are presented in Table 2.2 (p. 26) and Table 2.3 (p. 27), respectively, and derived energy equivalents are compared in Table 2.4 (p. 27) between both modes. Mean and standard deviation of mean for the experiments in the first mode is (1371.78 ± 0.29) $J \cdot K^{-1}$, while the corresponding values for the second mode is (1371.84 ± 0.25) $J \cdot K^{-1}$.

Auxiliary data for salicylic acid are given in Table 2.1 (p. 23). In this series, six combustion experiments were conducted. Results of the combustion experiments are given in Table 2.5 (p. 28). Mean and standard deviation of mean of standard molar enthalpy of combustion is $-(3023.67 \pm 0.28)$ $kJ \cdot mol^{-1}$. Derived standard molar enthalpies of combustion and of formation are presented and compared with reported data in Table 2.6 (p. 30). The present value agrees with most of the reported values at least within the sum of uncertainties.

2.5 Performance of the new calorimeter

The obtained temperature data of the initial and final periods are fitted to the function:

$$T = T_\infty - (T_\infty - T_0) \exp\{-k\,(t - t_0)\} \tag{2.6}$$

where T_∞ is the convergence temperature, t_0 and T_0 is the time and temperature at the beginning of the initial or final period, and k is the cooling constant of Newton's law. In Figure 2.4 of page 29, the scatter of temperature data from the fitted curves for the initial

Table 2.2: Results of calibration for salicylic acid with benzoic acid before electric energy correction

Exp. No.	1	2	3	4
m_B/mg	20.1102	19.3655	19.4021	20.4056
m(fuse)/mg	0.1730	0.2043	0.1778	0.1602
$n(HNO_3)/\mu$mol	0.760	0.437	0.760	1.340
ϵ^i/J·K^{-1}	0.358	0.357	0.357	0.358
ϵ^f/J·K^{-1}	0.381	0.379	0.379	0.381
T_i/ ℃	24.57855	24.57903	24.57789	24.57933
T_f/ ℃	25.08079	25.07095	25.06989	25.08724
ΔT_c/mK	61.11	64.28	63.52	60.32
ΔT_{ad}/mK	441.13	427.64	428.49	447.60
E_{ign}/J	0.120	0.116	0.117	0.111
E_{el}/J	65.200	65.391	66.304	67.637
$-\Delta_{IBP} U$/J	539.643	521.387	521.146	546.894
$\Delta U(HNO_3)$/J	0.045	0.026	0.045	0.080
$-m_B\Delta_c u$/J	531.183	511.513	512.479	538.935
ϵ°(comb)/J·K^{-1}	1371.03	1372.05	1370.91	1372.85

Exp. No.	5	6	7
m_B/mg	18.2461	20.6356	20.1853
m(fuse)/mg	0.2750	0.1670	0.0914
$n(HNO_3)/\mu$mol	2.173	1.078	0.998
ϵ^i/J·K^{-1}	0.356	0.358	0.358
ϵ^f/J·K^{-1}	0.376	0.382	0.381
T_i/ ℃	24.58101	24.57913	24.57853
T_f/ ℃	25.05954	25.09176	25.08167
ΔT_c/mK	68.01	59.17	61.22
ΔT_{ad}/mK	495.17	453.45	441.92
E_{ign}/J	0.132	0.129	0.112
E_{el}/J	68.262	68.841	68.087
$-\Delta_{IBP} U$/J	495.173	553.274	537.863
$\Delta U(HNO_3)$/J	0.130	0.064	0.060
$-m_B\Delta_c u$/J	481.945	545.060	533.166
ϵ°(comb)/J·K^{-1}	1372.67	1371.88	1371.07

m_B: Mass of benzoic acid. m(fuse): Mass of polyethylene fuse. $n(HNO_3)$: Amount of HNO_3 ϵ^i: Energy equivalent of the bomb contents in the initial state. ϵ^f: Energy equivalent of the bomb contents in the final state. T_i: Initial temperature of the reaction period. T_f: Final temperature of the reaction period. ΔT_c: Correction to the temperature rise. ΔT_{ad}: Adiabatic temperature rise. E_{ign}: Ignition energy. E_{el}: Electric energy to the internal microheater. IBP: Isothermal bomb process. $\Delta U(HNO_3)$: Energy change associated with the formation of HNO_3. ΔU_Σ: Standard-state correction. ϵ°: Energy equivalent of the standard calorimetric system (without the contents).

Table 2.3: Results of calibration for salicylic acid with the internal microheater before electric energy correction

Exp. No.	1	2	3	4
ϵ^{C}/J·K^{-1}	0.381	0.379	0.379	0.381
T_i/ ℃	24.57916	24.57915	24.57903	24.57233
T_f/ ℃	25.08719	25.08062	25.08449	25.08597
ΔT_c/mK	64.45	65.93	64.99	57.02
ΔT_{ad}/mK	443.57	435.54	440.47	456.62
E_{el}/J	608.238	597.648	604.252	626.998
ϵ°(el)/J·K^{-1}	1370.85	1371.84	1371.46	1372.75

Exp. No.	5	6	7
ϵ^{C}/J·K^{-1}	0.376	0.382	0.381
T_i/ ℃	24.57956	24.57798	24.57982
T_f/ ℃	25.09707	25.09328	25.08763
ΔT_c/mK	62.51	61.99	65.00
ΔT_{ad}/mK	455.00	453.30	442.80
E_{el}/J	624.116	622.035	607.204
ϵ°(el)/J·K^{-1}	1371.29	1371.84	1370.90

ϵ^{C}: Energy equivalent of the bomb contents. T_i: Initial temperature of the reaction period. T_f: Final temperature of the reaction period. ΔT_c: Correction to the temperature rise. ΔT_{ad}: Adiabatic temperature rise. E_{el}: Electric energy to the internal microheater. ϵ°(el): Energy equivalent of the standard calorimetric system (without the contents).

Table 2.4: Corrected energy equivalents

Exp. No.	1	2	3	4	5	6	7
ϵ°(comb)/J·K^{-1}	1371.06	1372.08	1370.94	1372.88	1372.51	1371.91	1371.10
ϵ°(el)/J·K^{-1}	1371.13	1372.12	1371.74	1373.03	1371.57	1372.12	1371.18

Table 2.5: Results of combustion calorimetry of salicylic acid

Exp. No.	1	2	3	4	5	6
m(compd.)/mg	23.6306	23.2181	23.4086	23.7677	24.0920	23.3705
m(fuse)/mg	0.2005	0.1560	0.1586	0.1859	0.2165	0.1010
$n(HNO_3)/\mu$mol	0.810	0.728	0.460	0.757	0.907	0.684
ϵ^{i}/J·K^{-1}	0.367	0.367	0.367	0.367	0.368	0.367
ϵ^{f}/J·K^{-1}	0.384	0.383	0.384	0.385	0.385	0.383
T_i/ ℃	24.57958	24.58013	24.57960	24.57954	24.58088	24.58051
T_f/ ℃	25.07599	25.07064	25.07160	25.07990	25.08513	25.07105
ΔT_c/mK	62.48	64.32	64.42	62.61	62.84	64.66
ΔT_{ad}/mK	433.93	426.20	427.57	437.74	441.40	425.87
E_{ign}/J	0.111	0.121	0.121	0.151	0.151	0.128
E_{el}/J	68.177	68.597	66.245	71.199	67.720	67.342
$-\Delta_{IBP}U$/J	527.129	516.091	520.327	529.297	537.795	516.891
$\Delta U(HNO_3)$/J	0.048	0.043	0.027	0.045	0.054	0.041
ΔU_Σ/J	0.456	0.447	0.451	0.459	0.466	0.449
$-\Delta_c u°$(c)/J·g^{-1}	21892.8	21895.7	21893.9	21886.2	21884.8	21896.2
$-\Delta_c U°$(c)/kJ·mol^{-1}	3023.84	3024.24	3023.98	3022.92	3022.73	3024.30

m(compd.): Sample mass. m(fuse): Mass of polyethylene fuse. $n(HNO_3)$: Amount of HNO_3 ϵ^{i}: Energy equivalent of the bomb contents in the Initial state. ϵ^{f}: Energy equivalent of the bomb contents in the final state. T_i: Initial temperature of the reaction period. T_f: Final temperature of the reaction period. ΔT_c: Correction to the temperature rise. ΔT_{ad}: Adiabatic temperature rise. E_{ign}: Ignition energy. E_{el}: Electric energy to the internal microheater. IBP: Isothermal bomb process. $\Delta U(HNO_3)$: Energy change associated with the formation of HNO_3. ΔU_Σ: Standard-state correction. $\Delta_c u°$(c): Standard specific energy of combustion. $\Delta_c U°$(c): Standard molar energy of combustion.

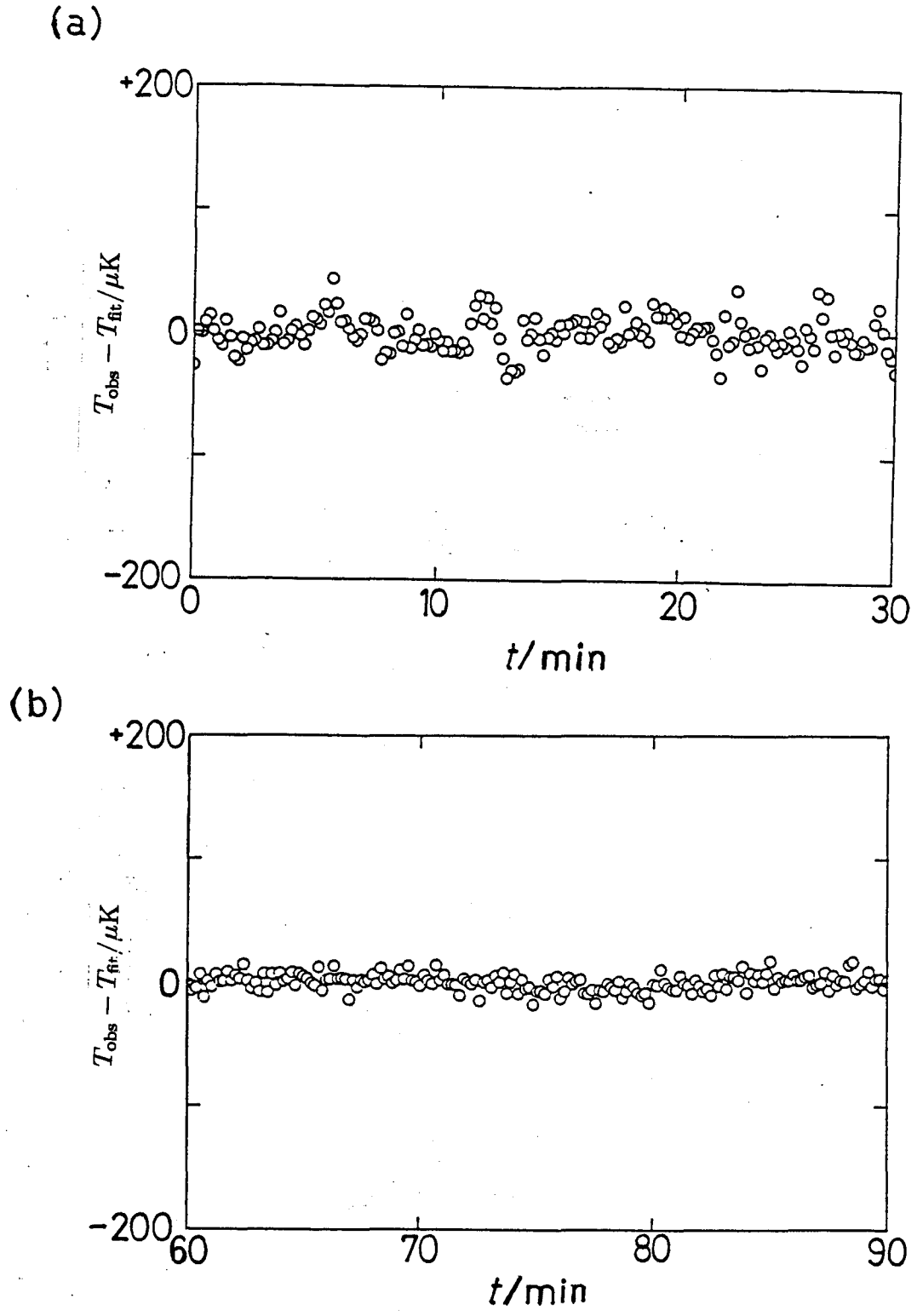

(a)Initial period. (b)Final period.

Figure 2.4: Scatter of the temperature data from smoothed curves

Table 2.6: Standard thermodynamic quantities of salicylic acid. Comparison with reported values.

Reference	$-\Delta_c u°$(c)	$-\Delta_f H°$(c)
The present work	21891.6±5.1	588.4±1.7
Diogo *et al.*[17]	21895±4	587.8±1.5
Beckers [23] [45]	21887±5	588.9±1.5
Keffler [23] [46]	21881±4	589.9±1.0
Stiehler *et al.* [23] [47]	21880±4	589.9±1.0
Milone *et al.* [23] [48]	21846±10	594.5±2.9
Badoche [23] [49]	21886±10	589.1±3.0
Sabbah *et al.* [15b]	21908±7	586.1±1.9

The uncertainties for $\Delta_c u°$ and $\Delta_f H°$ are the standard deviation of the mean and twice the standard deviation of the mean, respectively.

and final periods is shown. Most of the scattered data is within ±50 μK and ±25 μK for initial and final periods, respectively.

In Figure 2.5 (p. 31), the potential difference across the microheater plus lead wires, the current flowing through it, and the electric power and resistance derived from these are plotted against time for an experiment of calibration of electric energy.

The electric potential and current for the ignition circuit measured by the oscilloscope are shown in Figure 2.6(a) (p. 32), and the electric power and resistance are shown in Figure 2.6(b).

Simultaneous measurement of both potential difference and current enables us to determine the temperature change of the microheater. In Figure 2.7 (p. 33), the variation of the resitance of the microheater plus lead wires with time is shown for the combustion of a polyethylene pellet either with or without electric power supply of a proper magnitude to the microheater. In the case of the experiment without the power supply, an electric current of 10 mA was used to detect the resistance change, while in the case of experiment with the power supply, the same intensity (10 mA) of electric current was used before and after the proper power supply. Decrease in the rate of temperature change after the highest temperature detected is clearly observed.

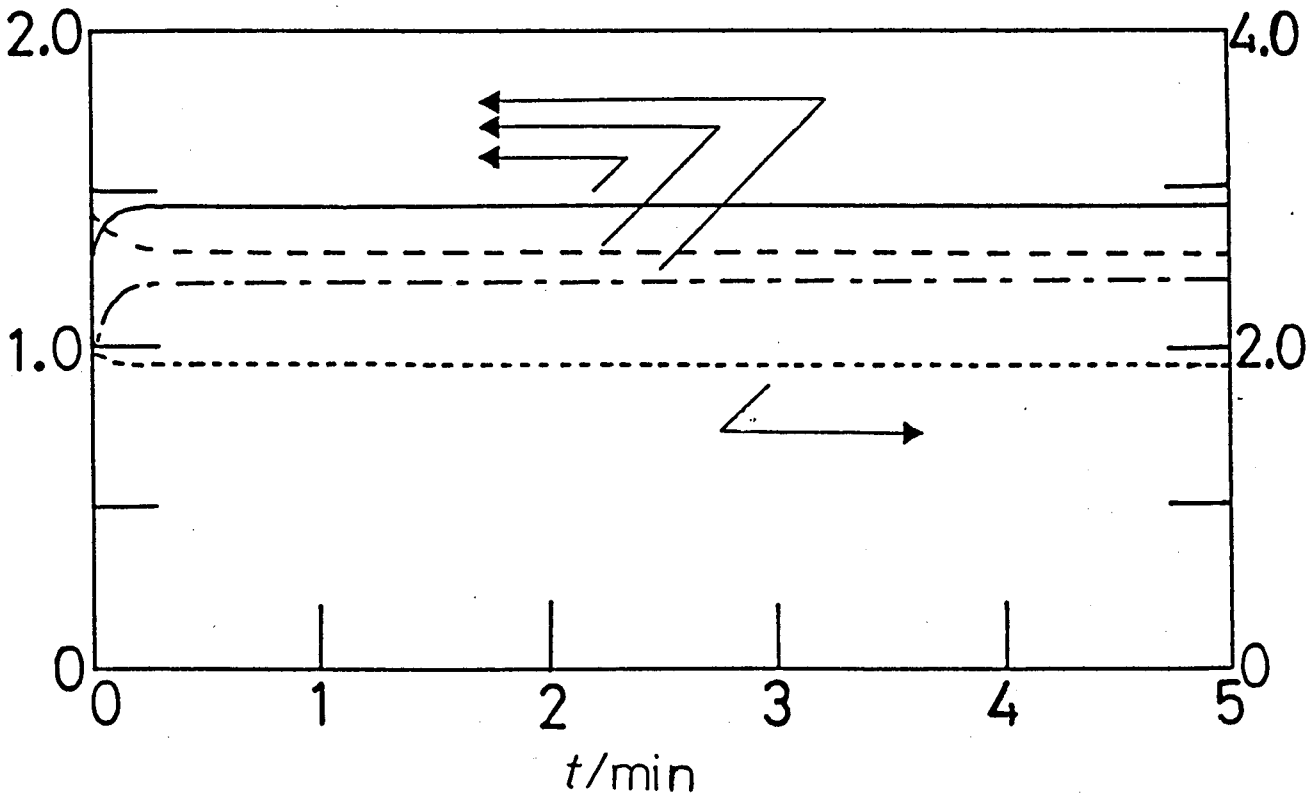

— :Potential/V, – – :Current/A, – - – :Resistance(R/R_0), - - - - :Power/W

Figure 2.5: Electric potential, current, resistance and power for microheater for a calibration experiment of electric energy

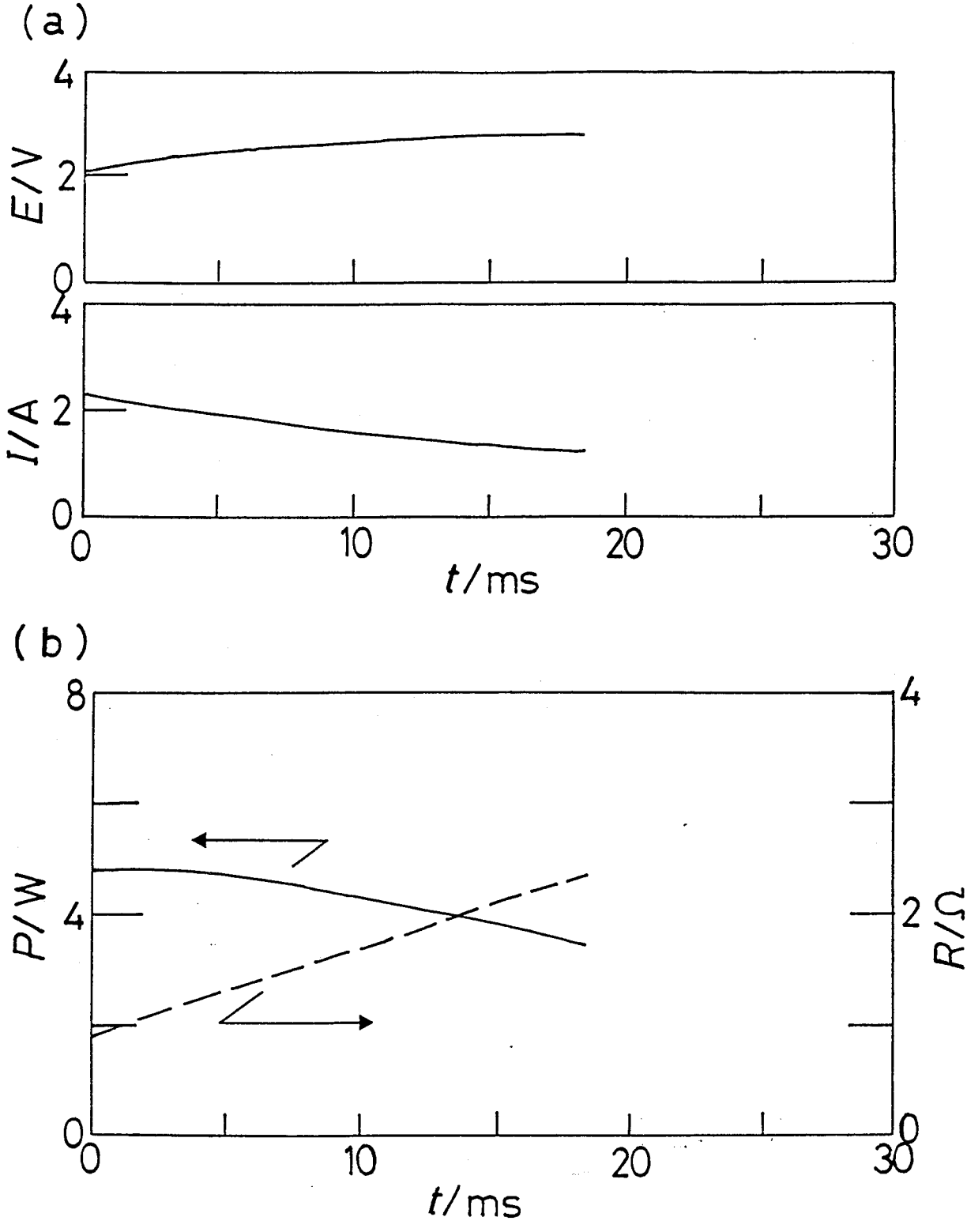

Figure 2.6: Electric potential, current, resistance and power for ignition

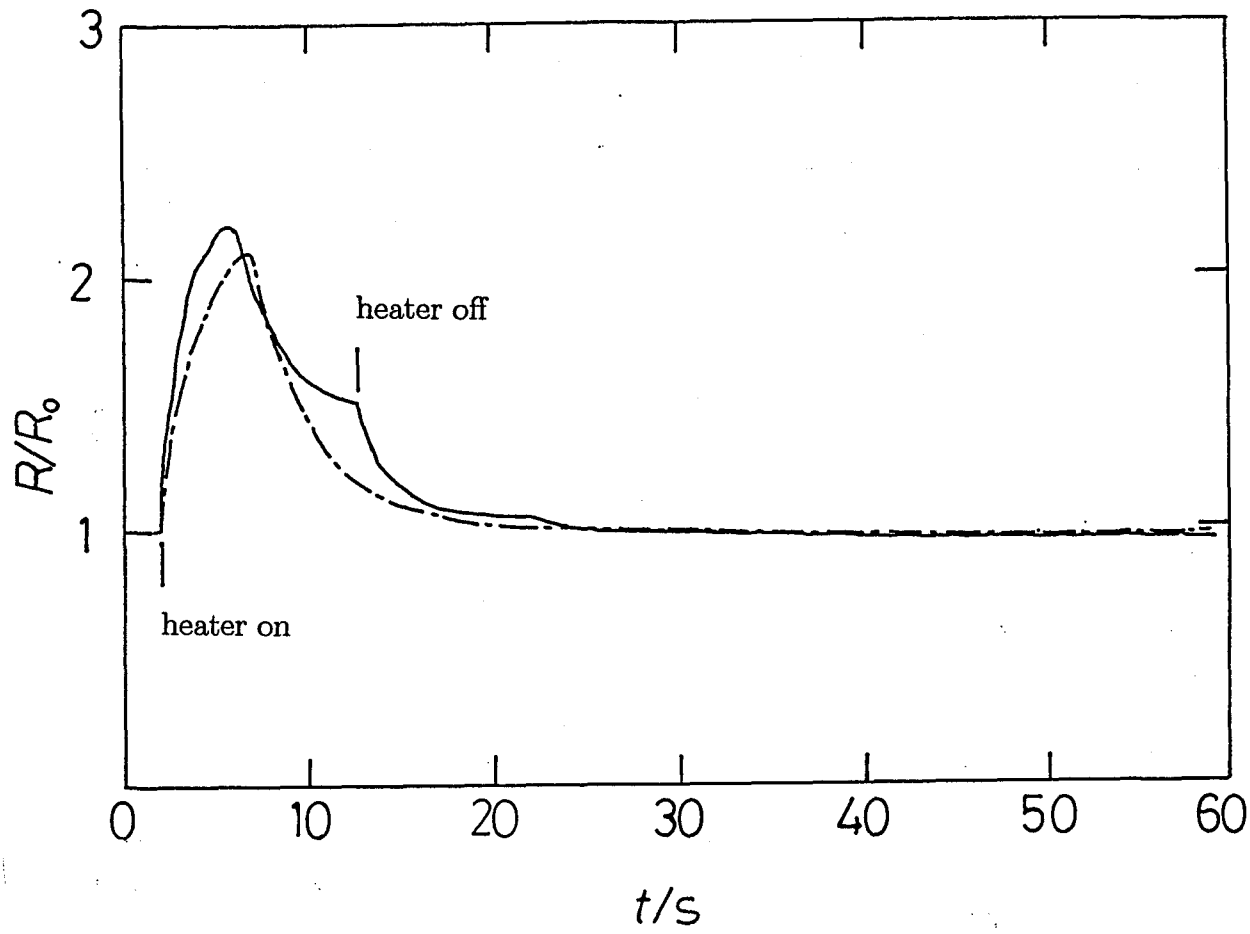

Polyethylene 6.5mg. — :With heating. – – :Without heating.

Figure 2.7: Resistance of microheater during combustion – how microheater works

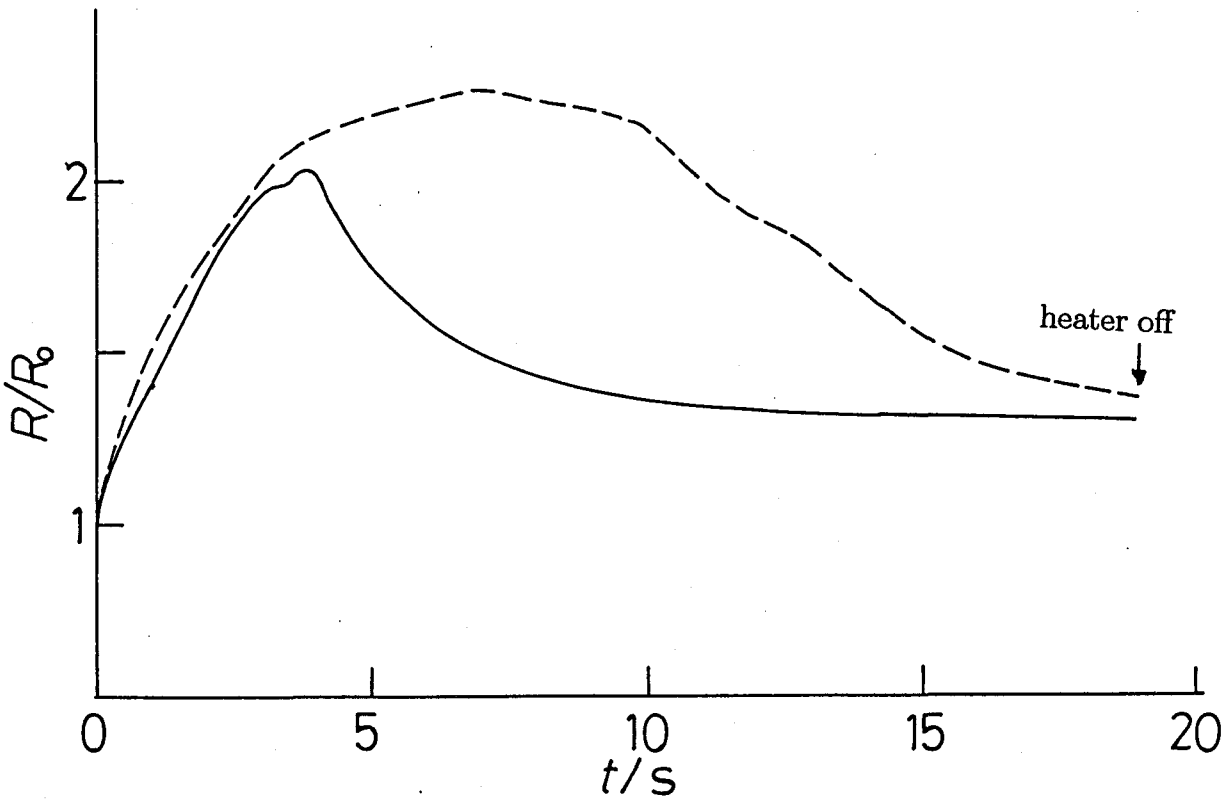

— :Benzoic acid. – – :Coronene.

Figure 2.8: Resistance of microheater during combustion – sample dependency

In Figure 2.8 (p. 34), the variations of the resistance of the microheater with time in the actual calorimetric measurements are compared between more and less readily combustible substances (benzoic acid and coronene, respectively). For less readily combustible compounds, longer time was required for combustion and hence, in some cases the length of power supply should be extended.

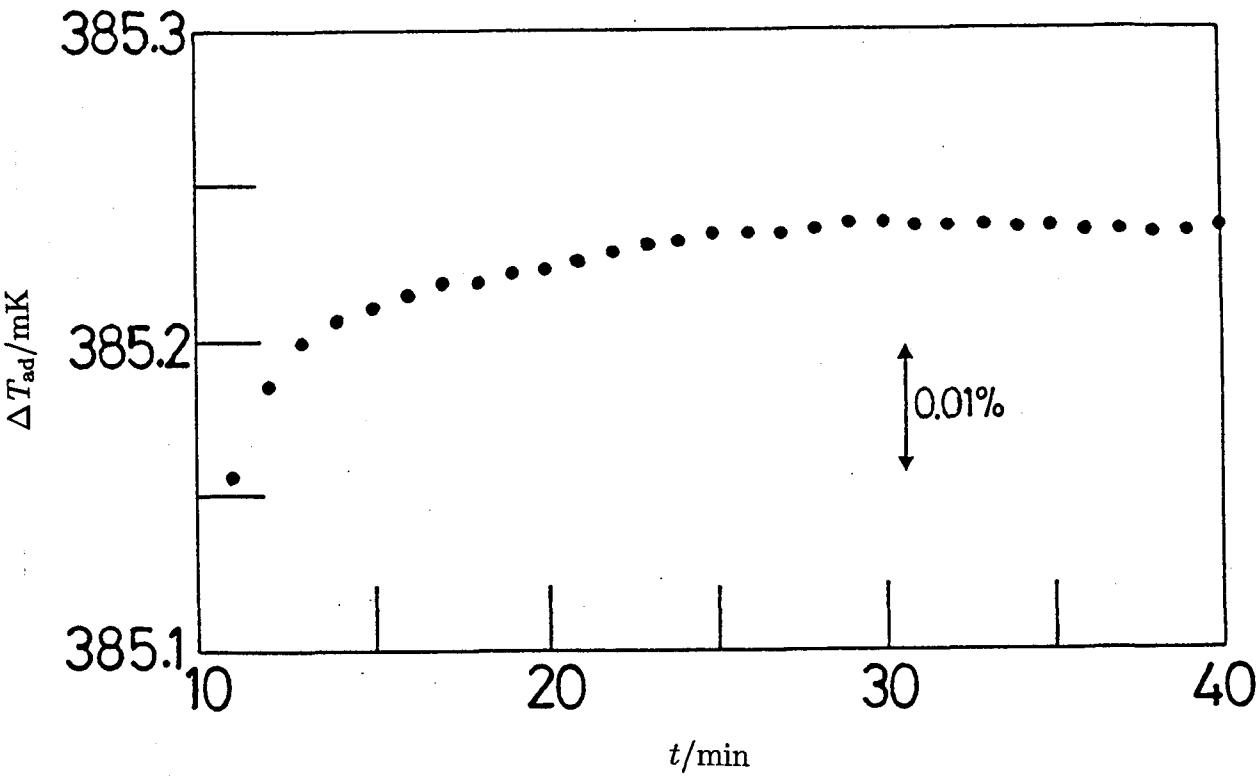

Figure 2.9: Calculated adiabatic temperature rise as a function of reaction period
The lengths of the initial and final periods are fixed to 30 min.

In Figure 2.9, the adiabatic temperature rise is shown as a function of the length of the reaction period. For the length of reaction period longer than 25 min, the adaibatic temperature rise is constant within ±0.005 %. The choice of 30 min for the usual length of reaction period is based on this result. In the present bomb, a larger amount of thermal insulator materials is used as compared with ordinary combustion calorimeters. It should,

therefore, be considered quite fortunate that a reaction period of 30 min length is sufficient for becoming thermally stationary after a combustion or electrical heating.

Chapter 3

Combustion Calorimetry of C_{60} and C_{70} *

3.1 Introduction

To evaluate the energetic stability of fullerenes, the determination of standard enthalpy of formation by oxygen bomb combustion calorimetry is one of the sophisticated methods. However, partly because of the difficulties in obtaining a large amount of pure fullerenes and in realizing complete combustion, few calorimetric studies have been reported. Recently, the author constructed an isoperibol micro-bomb combustion calorimeter with a miniature combustion bomb of novel design which requires only 10~20 mg of a sample per combustion. In the present work, combustion calorimetry on C_{60} and C_{70} was accomplished by use of this calorimeter and the standard enthalpies of formation, which is a measure of relative stabilities with reference to graphite, were determined. For C_{70}, this is the first experimental determination of the formation enthalpy.

3.2 Experimental

Sample

The samples of C_{60} and C_{70} were supplied by Prof. T. Atake at Tokyo Institute of Technology [22] and used in this study without further purification. By mass spectroscopic analysis, other fullerene species were detected in a barely recognizable amount in the C_{60}

*The main part of this chapter was published in Kiyobayashi, T. ; Sakiyama, M. *Full. Sci. Technol.* **1993**, *1*, 269-273.

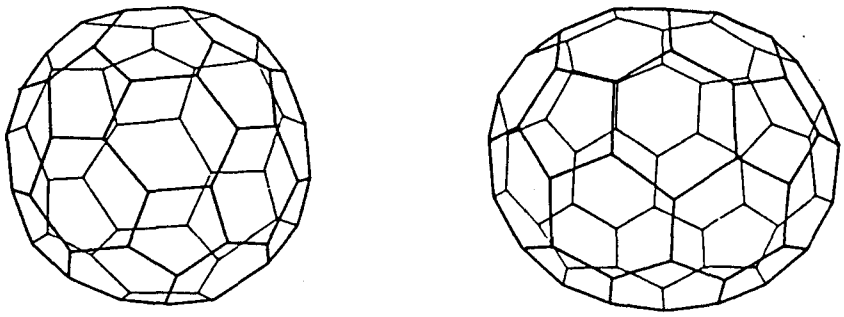

Figure 3.1: C_{60} and C_{70}

sample, while C_{60} was found to be present in the C_{70} sample by 7 wt% (s. Fig 3.2). ^{1}H NMR analysis showed that both the C_{60} and C_{70} samples were contaminated with 0.26 wt% of benzene.

Calibration of Calorimeter

The energy equivalent of the empty calorimeter and a correction factor f for the measured electric energy supplied to the internal microheater were determined by burning thermochemical standard benzoic acid (NIST SRM 39i; $\Delta_c u_{cert} = -26434$ J·g^{-1}) under certificate conditions. Electric energy for the ignition was measured separately. The mean and standard deviation of the mean of the observed energy equivalents was (1374.68 ± 0.16) J·K^{-1} from five calibration runs (s. Table 3.1). The correction factor f for the measured electric energy was determined to be (1.00052 ± 0.00030).

Combustion Calorimetry

Table 3.2 shows the results of combustion calorimetry on C_{60} and C_{70}. The samples were formed into pellets and ignited under the oxygen pressure of 3.04 MPa in the presence of 24 mg of water in the combustion bomb with an internal volume of 9 cm^3. To the internal microheater, electric energies of 100 J and 200 J were supplied in the case of C_{60} and C_{70},

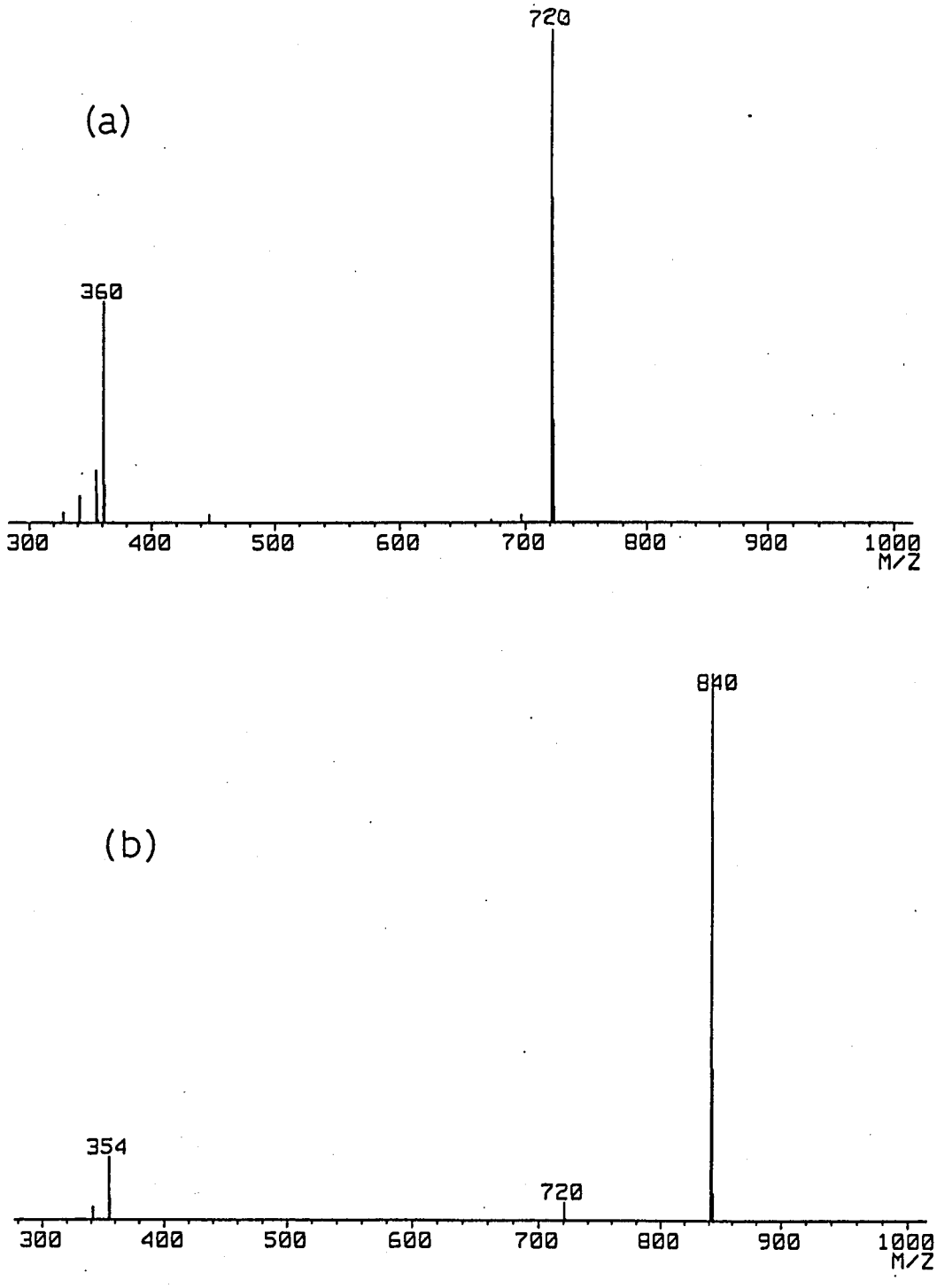

Figure 3.2: Mass spectra of (a):C_{60} and (b):C_{70}.

Table 3.1: Results of calibration for C_{60} and C_{70} with benzoic acid

Exp. No.	1	2	3	4	5
m_B/mg	20.1716	20.0676	18.4393	20.8690	21.3098
m(fuse)/mg	0.1122	0.1031	0.1144	0.1177	0.1430
$n(HNO_3)/\mu$mol	0.601	0.384	0.722	0.864	0.515
ϵ^i/J·K^{-1}	0.358	0.357	0.356	0.358	0.359
ϵ^f/J·K^{-1}	0.381	0.380	0.377	0.382	0.383
T_i/ ℃	24.58144	24.58126	24.58618	24.58629	24.58470
T_f/ ℃	25.10701	25.10569	25.08940	25.12834	25.13363
ΔT_c/mK	58.90	59.65	67.64	59.87	56.86
ΔT_{ad}/mK	466.67	464.78	435.584	482.174	492.067
E_{ign}/J	0.071	0.103	0.051	0.092	0.109
E_{el}/J	103.266	103.713	106.340	105.561	106.450
$-\Delta_{IBP} U$/J	538.445	535.260	492.758	557.152	569.956
$\Delta U(HNO_3)$/J	0.036	0.023	0.043	0.052	0.031
$-m_B \Delta_c u$/J	532.805	530.056	487.049	551.225	562.869
ϵ°/J·K^{-1}	1374.87	1374.64	1375.15	1374.25	1374.48

m_B: Mass of benzoic acid. m(fuse): Mass of polyethylene fuse. $n(HNO_3)$: Amount of HNO_3 ϵ^i: Energy equivalent of the bomb contents in the initial state. ϵ^f: Energy equivalent of the bomb contents in the final state. T_i: Initial temperature of the reaction period. T_f: Final temperature of the reaction period. ΔT_c: Correction to the temperature rise. ΔT_{ad}: Adiabatic temperature rise. E_{ign}: Ignition energy. E_{el}: Electric energy to the internal microheater. IBP: Isothermal bomb process. $\Delta U(HNO_3)$: Energy change associated with the formation of HNO_3. ΔU_Σ: Standard-state correction. ϵ°: Energy equivalent of the standard calorimetric system (without the contents).

respectively. No carbon soot was detected by visual observation of the crucible and no carbon monoxide was detected in the bomb gas after the experiment. A small amount of nitric acid, which was formed by oxidation of nitrogen contained in the oxygen gas as an impurity, was detected in the bomb solution after combustion experiments. However, the energy of formation of the nitric acid was found to give no significant effect to the energy of combustion. The density and specific heat capacity, used for the correction of weighing in air to masses and the reduction of experimental results to the standard state values, were taken to be 1.67 g·cm^{-3} and 0.765 J·K^{-1}g^{-1} respectively, for both C_{60} and C_{70} [25]. Standard specific energy of combustion of polyethylene used as a fuse was −46305 J·g^{-1} .

The effect of the benzene contamination was corrected by using a reported data [23] ; $\Delta_c u°$(benzene)/J·g^{-1} = −41830. For C_{70}, the contribution to the combustion energy from C_{60} was taken into account.

3.3 Results and Discussion

Derived results are as follows: $-\Delta_c u°$(c)/J·g^{-1} = 35907.7, 35919.3, 35919.8, 35908.6, and 35928.1 for C_{60} and 35593.9, 35573.2, and 35572.3 for C_{70}. The mean and standard deviation of the mean are (35916.7 ± 3.8) and (35579.8 ± 7.1) for C_{60} and C_{70}, respectively.

Standard thermodynamic quantities of C_{60} and C_{70} are shown in Table 3.3. The values of $\Delta_c U°$(s) and $\Delta_f H°$(s) in Table 3.3 refer to the following reactions, respectively.

$$C_n(c) + nO_2(g) \longrightarrow nCO_2(g)$$

$$nC(\text{graphite}) \longrightarrow C_n(c)$$

In calculating the $\Delta_f H°$ values, the CODATA recommended standard enthalpy of formation for CO_2(g), −(393.51 ± 0.13) kJ·mol^{-1} , was used [4]. Uncertainties given in Table 3.3 are twice the final overall standard deviations of the mean.

The derived result for C_{60} is compared with the reported values in Table 3.4. The present value agrees with that obtained by Beckhaus *et al.* [24] and Diogo *et al.* [36].

Comparison of $\Delta_f H°(C_n, s)/n$, which is the standard enthalpy of formation reduced to 12.011 g of carbon, between C_{60} and C_{70} shows that C_{70}(s) is significantly more stable than C_{60}(s).

Table 3.2: Results of combustion calorimetry of C_{60} and C_{70}

— C_{60} —

Exp. No.	1	2	3	4	5
m(compd.)/mg	12.9654	13.4512	14.0371	12.4867	14.6049
m(fuse)/mg	0.1268	0.2006	0.1859	0.1817	0.1688
$n(HNO_3)/\mu$mol	0.784	0.643	0.743	0.963	0.784
ϵ^i/J·K^{-1}	0.343	0.344	0.344	0.343	0.345
ϵ^f/J·K^{-1}	0.345	0.345	0.346	0.344	0.346
T_i/ ℃	24.58607	24.58477	24.58561	24.58538	24.58557
T_f/ ℃	25.07176	25.08398	25.09802	25.06240	25.10778
ΔT_c/mK	72.34	68.37	67.18	73.21	63.44
ΔT_{ad}/mK	413.35	430.83	445.23	403.81	458.76
E_{ign}/J	0.102	0.082	0.133	0.134	0.125
E_{el}/J	99.551	99.227	98.565	97.690	97.423
$-\Delta_{IBP} U$/J	468.712	493.099	513.506	457.418	533.262
$\Delta U(HNO_3)$/J	0.047	0.038	0.044	0.057	0.047
ΔU_Σ/J	0.387	0.407	0.426	0.376	0.445
$-\Delta_c u°$(c)/J·g^{-1}	35907.7	35919.3	35919.8	35908.6	35928.1
$-\Delta_c U°$(c)/kJ·mol^{-1}	25877.3	25885.6	25886.0	25877.9	25892.0

— C_{70} —

Exp. No.	1	2	3
m(compd.)/mg	11.3888	12.4133	8.8377
m(fuse)/mg	0.2142	0.2085	0.1374
$n(HNO_3)/\mu$mol	0.474	0.962	0.884
ϵ^i/J·K^{-1}	0.342	0.343	0.340
ϵ^f/J·K^{-1}	0.344	0.344	0.341
T_i/ ℃	24.58877	24.58769	24.58884
T_f/ ℃	25.10269	25.12159	25.04664
ΔT_c/mK	69.06	63.52	80.86
ΔT_{ad}/mK	444.87	470.38	376.93
E_{ign}/J	0.104	0.095	0.120
E_{el}/J	195.496	194.527	196.761
$-\Delta_{IBP} U$/J	416.100	452.167	321.409
$\Delta U(HNO_3)$/J	0.028	0.057	0.053
ΔU_Σ/J	0.341	0.374	0.260
$-\Delta_c u°$(c)/J·g^{-1}	35593.9	35573.2	35572.3
$-\Delta_c U°$(c)/kJ·mol^{-1}	29926.3	29908.9	29908.1

m(compd.): Sample mass. m(fuse): Mass of polyethylene fuse. ΔT_{ad}: Adiabatic temperature rise. E_{ign}: Ignition energy. E_{el}: Electric energy to the internal microheater. IBP: Isothermal bomb process. $\Delta_c u°$(c): Standard specific energy of combustion. $\Delta_c U°$(c): Standard molar energy of combustion.

Table 3.3: Standard thermodynamic quantities of C_{60} and C_{70} at 298.15 K

	C_{60}	C_{70}
$\Delta_c u°(c)=\Delta_c h°(c)/J\cdot g^{-1}$	−35917±18	−35580±20
$\Delta_c U°(c)=\Delta_c H°(c)/kJ\cdot mol^{-1}$	−25884±13	−29914±16
$\Delta_f H°(c)/kJ\cdot mol^{-1}$	2273±15	2369±18
$(\Delta_f H°(c)/n)/kJ\cdot mol(C)^{-1}$	37.89±0.25	33.84±0.26

Table 3.4: Comparison of the results of this work for C_{60} with reported values.

	$\Delta_c u°(c)/J\cdot g^{-1}$	$\Delta_f H°(c)/kJ\cdot mol^{-1}$
This work	−35917±18	2273±15
Kolesov *et al.* [50]	−36030±16	2355±15
Beckhaus *et al.* [35]	−35990±22	2327±17
Diogo *et al.* [36]	−35923±17	2278±14
Beckhaus *et al.* [24]	−35929.5±5.7	2282.5±8.8
Steele *et al.* [25]	−36123.7±9.7	2422±10

In the present study, correction was made for the contribution of impurities. However, it is more desirable measure the samples of higher purity. The author wish to perform a new series of measurements for highly purified samples and also for samples of other fullerenes. The use of a small amount of samples, *ca.* 13 mg per combustion, is the merit of the present method, and the method is convenient for samples of a limited quantity.

The author are sincerely grateful to Prof. Tooru Atake for a gift of C_{60} and C_{70}.

Chapter 4

Combustion Calorimetry of Corannulene *

4.1 Introduction

The remarkable yield of fullerenes and carbon nanotubes in arc-discharge experiments has raised fundamental questions about the stability of non-planar polycyclic aromatic hydrocarbons (PAHs) and carbon sheets. Enthalpies of formation of such systems provide the best quantitative measures of the thermodynamic stabilities they enjoy and the strains from which they suffer; however, experimental data in this area remain sparse. Corannulene [Figure 4.1], a bowl-shaped $C_{20}H_{10}$ hydrocarbon, represents the minimal fragment of a fullerene that retains the characteristic curvature. Herein we report our results from micro-bomb combustion calorimetry on corannulene and the first experimentally-based enthalpy of formation for this key compound.

4.2 Experimental

Sample

The original synthesis of corannulene, reported by Barth and Lawton in 1966 [26], gave sufficient quantities of corannulene for X-ray analysis and for a variety of spectroscopic studies but not enough for calorimetric research. Fortunately new synthetic strategies have finally made corannulene available in significantly larger quantities [27]. For the

*The main part of this chapter was published in Kiyobayashi, T. ; Nagano, Y. ; Sakiyama, M. ; Yamamoto, K. ; Cheng, P.-C. ; Scott, L. T. *J. Am. Chem. Soc.* **1995**, *117*, 3270-3271.

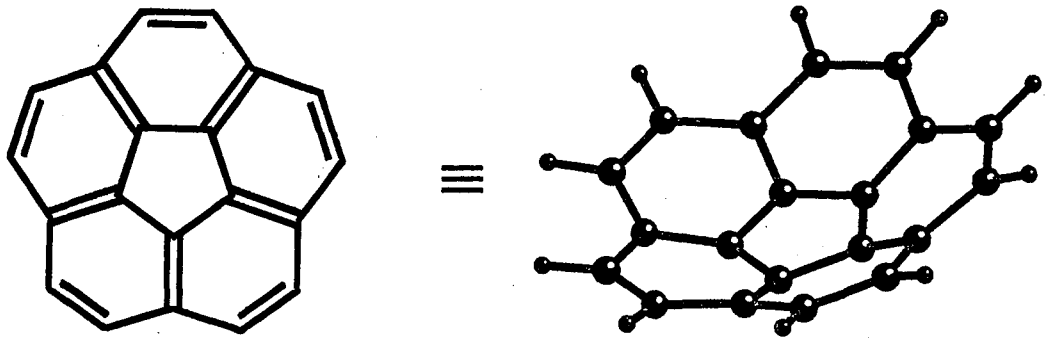

Figure 4.1: Corannulene $C_{20}H_{10}$

work described here, corannulene was prepared by flash vacuum pyrolysis of 7,10-di(1-chlorovinyl)fluoranthene [27d, 27e]. Material obtained in this manner, though pure by ^{1}H NMR spectroscopy, was shown by capillary GC/MS and analytical HPLC to contain trace amounts of chlorocorannulene, a contaminant formed in the pyrolysis. Repeated chromatography on silica gel and recrystallization ultimately gave pure corannulene.

Calibration of Calorimeter

The energy equivalent of the empty calorimeter and a correction factor f for the measured electric energy supplied to the internal microheater were determined by burning 20 mg of thermochemical standard benzoic acid (NIST SRM 39i; $\Delta_c u_{cert} = -26434$ J·g^{-1}) under certificate conditions. The results of the calibration are given in Table 4.1. The mean and standard deviation of the mean of the observed energy equivalents was (1378.94 ± 0.27) J·K^{-1} from six calibration runs. The correction factor f for the measured electric energy was determined to be (0.99897 ± 0.00017).

Combustion Calorimetry of Corannulene

The corannulene sample was formed into *ca.* 14 mg pellets for each combustion and burned under an oxygen pressure of 3.04 MPa in the presence of 24 mg of water in the micro-bomb.

Table 4.1: Results of calibration for corannulene with benzoic acid

Exp. No.	1	2	3	4	5
m_B/mg	19.9072	20.1388	20.6387	19.1123	19.8121
m(fuse)/mg	0.1166	0.2144	0.1594	0.2306	0.1410
$n(HNO_3)/\mu$mol	1.496	0.882	0.701	1.044	0.924
ϵ^i/J·K^{-1}	0.357	0.358	0.358	0.357	0.357
ϵ^f/J·K^{-1}	0.380	0.381	0.382	0.378	0.380
T_i/ ℃	24.59289	24.59428	24.59230	24.59279	24.59411
T_f/ ℃	25.11749	25.12463	25.12830	25.10726	25.11837
ΔT_c/mK	70.68	70.72	68.46	72.91	72.07
ΔT_{ad}/mK	453.927	459.636	467.545	441.555	452.194
E_{ign}/J	0.094	0.090	0.111	0.136	0.173
E_{el}/J	93.626	91.582	92.104	92.628	92.877
$-\Delta_{IBP}U$/J	531.712	542.328	552.985	515.952	530.294
$\Delta U(HNO_3)$/J	0.089	0.053	0.042	0.062	0.055
$-m_B\Delta_c u$/J	525.821	531.938	545.142	504.825	523.309
ϵ°/J·K^{-1}	1377.47	1378.99	1379.61	1378.21	1378.13

Exp. No.	6	7	8	9	10
m_B/mg	18.0191	20.5443	21.5059	10.0615	20.5325
m(fuse)/mg	0.1693	0.1541	0.1171	0.1372	0.1017
$n(HNO_3)/\mu$mol	0.871	0.885	2.338	0.536	1.426
ϵ^i/J·K^{-1}	0.355	0.358	0.359	0.346	0.358
ϵ^f/J·K^{-1}	0.376	0.382	0.384	0.357	0.381
T_i/ ℃	24.59117	24.59366	24.58739	24.58648	24.58633
T_f/ ℃	25.08418	25.12933	25.13016	24.95156	25.11387
ΔT_c/mK	75.76	69.00	60.53	100.34	63.64
ΔT_{ad}/mK	417.258	466.662	482.238	264.733	463.908
E_{ign}/J	0.144	0.102	0.117	0.100	0.115
E_{el}/J	91.443	93.410	90.940	92.816	91.828
$-\Delta_{IBP}U$/J	484.202	550.255	574.049	272.338	547.548
$\Delta U(HNO_3)$/J	0.052	0.053	0.140	0.032	0.085
$-m_B\Delta_c u$/J	525.821	542.649	568.048	265.760	542.337
ϵ°/J·K^{-1}	1379.58	1379.15	1378.85	1379.36	1378.13

m_B: Mass of benzoic acid. m(fuse): Mass of polyethylene fuse. $n(HNO_3)$: Amount of HNO_3 ϵ^i: Energy equivalent of the bomb contents in the initial state. ϵ^f: Energy equivalent of the bomb contents in the final state. T_i: Initial temperature of the reaction period. T_f: Final temperature of the reaction period. ΔT_c: Correction to the temperature rise. ΔT_{ad}: Adiabatic temperature rise. E_{ign}: Ignition energy. E_{el}: Electric energy to the internal microheater. IBP: Isothermal bomb process. $\Delta U(HNO_3)$: Energy change associated with the formation of HNO_3. ΔU_Σ: Standard-state correction. ϵ°: Energy equivalent of the standard calorimetric system (without the contents).

On each combustion run, 90 J of electric energy was supplied to the internal microheater to achieve complete combustion. No carbon soot was detected by visual observation of the crucible. No carbon monoxide was detected from the bomb gas after combustion. The amount of nitric acid, which was formed by the oxidation of nitrogen impurity contained in the oxygen gas, was determined by UV spectrometry of the bomb solution. The contribution of enthalpies of formation and solution of the nitric acid to the calorimetry were taken into account. The density and specific heat capacity of corannulene were taken to be 1.31 $g \cdot cm^{-3}$ from the crystal structure in ref [29] and 1.045 $J \cdot K^{-1} g^{-1}$, respectively, for the buoyancy correction and the reduction of the experimental results to the standard state values. Standard specific energy of combustion, $\Delta_c u°$, of polyethylene fuse was -46305 $J \cdot g^{-1}$.

Results of six combustion runs are collected in Table 4.2. The mean value and standard deviation of the mean are -38496.0 and 7.6 $J \cdot g^{-1}$, respectively.

4.3 Result

Standard thermodynamic quantities of corannulene are shown in Table 4.3. Reduction to standard state was carried out by following the literature procedure [3]. The values of $\Delta_c U°(c)$ and $\Delta_f H°(c)$ refer to the following reactions, respectively.

$$C_{20}H_{10}(c) + 22.5O_2(g) \longrightarrow 20CO_2(g) + 5H_2O(l)$$

$$20C(\text{graphite}) + 5H_2(g) \longrightarrow C_{20}H_{10}(c)$$

For calculation of $\Delta_f H°(c)$ value, the CODATA recommended standard formation enthalpy of $CO_2(g)$ $-(393.51 \pm 0.13)$ $kJ \cdot mol^{-1}$ and of $H_2O(g)$ $-(285.830 \pm 0.042)$ $kJ \cdot mol^{-1}$ were used [4]. Uncertainties are twice the final overall standard deviation of the mean according to the rule of error propagation.

In order to obtain the formation enthalpy in the gaseous state, we must determine the sublimation enthalpy. So far, no experimental value of the sublimation enthalpy of corannulene has been available. In Table 4.3, we show the sublimation enthalpy estimated by using an empirical non bonded atom-atom potential proposed by Williams [28b] on the basis of crystal structure determined by X-ray diffraction [29]. We also estimated the contribution

Table 4.2: Results of combustion calorimetry of corannulene

Exp. No.	1	2	3	4	5	6
m(compd.)/mg	15.3160	12.6067	13.7959	12.1777	11.4265	6.7699
m(fuse)/mg	0.1201	0.1805	0.1902	0.1596	0.1308	0.1601
$n(HNO_3)/\mu$mol	0.903	1.285	0.502	0.890	0.833	0.528
ϵ^i/J·K^{-1}	0.362	0.359	0.360	0.359	0.358	0.353
ϵ^f/J·K^{-1}	0.378	0.372	0.375	0.372	0.370	0.360
T_i/ ℃	24.59462	24.59557	24.58974	24.59372	24.58794	24.58807
T_f/ ℃	25.15225	25.09730	25.11128	25.08027	25.05376	24.95959
ΔT_c/mK	64.49	77.83	68.67	80.08	77.82	100.04
ΔT_{ad}/mK	493.142	423.903	452.870	406.471	388.001	271.475
E_{ign}/J	0.093	0.143	0.122	0.123	0.089	0.111
E_{el}/J	84.715	90.133	84.135	83.823	88.996	106.120
$-\Delta_{IBP} U$/J	595.384	494.413	540.389	476.700	446.022	268.168
$\Delta U(HNO_3)$/J	0.054	0.077	0.030	0.053	0.050	0.032
ΔU_Σ/J	0.405	0.328	0.362	0.315	0.294	0.169
$-\Delta_c u°$(c)/J·g^{-1}	38480.3	38523.2	38503.4	38508.2	38473.9	38487.1
$-\Delta_c U°$(c)/kJ·mol^{-1}	9631.6	9642.3	9637.4	9638.6	9630.0	9633.3

m(compd.): Sample mass. m(fuse): Mass of polyethylene fuse. $n(HNO_3)$: Amount of HNO_3 ϵ^i: Energy equivalent of the bomb contents in the Initial state. ϵ^f: Energy equivalent of the bomb contents in the final state. T_i: Initial temperature of the reaction period. T_f: Final temperature of the reaction period. ΔT_c: Correction to the temperature rise. ΔT_{ad}: Adiabatic temperature rise. E_{ign}: Ignition energy. E_{el}: Electric energy to the internal microheater. IBP: Isothermal bomb process. $\Delta U(HNO_3)$: Energy change associated with the formation of HNO_3. ΔU_Σ: Standard-state correction. $\Delta_c u°$(c): Standard specific energy of combustion. $\Delta_c U°$(c): Standard molar energy of combustion.

of dipole-dipole interaction to sublimation enthalpy with the dipole moment 2.433 Debye calculated by MOPAC v.6.03 with the PM3 Hamiltonian [30, 31]. Although this magnitude of dipole moment seems to be over-estimated, its contribution was found to be less than 1 kJ·mol^{-1} and was safely ignored. Interestingly, the sublimation enthalpy of corannulene estimated by the Williams empirical potentials agrees well with a simple empirical equation for planar PAH, $\Delta_{sub}H°$/kJ·mol^{-1} = 6.28n + RT, where n is the number of carbon atoms per molecule [33].

Table 4.3: Standard thermodynamic quantities of corannulene at 298.15K.

$\Delta_c u°$(c)/J·g^{-1}	−38496±22
$\Delta_c U°$(c)/kJ·mol^{-1}	−9635.5±5.4
$\Delta_c H°$(c)/kJ·mol^{-1}	−9641.7±5.4
$\Delta_f H°$(c)/kJ·mol^{-1}	342.3±5.6
$\Delta_{sub} H°$(c)/kJ·mol^{-1}	121.4*
$\Delta_f H°$(g)/kJ·mol^{-1}	463.7

* Estimated by empirical atom-atom potential in ref [28b] with crystal structure in ref [29].

4.4 Experimental and Theoretical $\Delta_f H°$

In Table 4.4 we show the comparisons among the formation enthalpies of corannulene, C_{60} and C_{70} derived by experiments and by various theoretical methods. As a general observation, ab initio methods with large scale basis sets, such as 6-31G*, and molecular mechanics provide better results for these non-planar systems than do the semi-empirical methods. The latter should improve in the next round of refinements, however, now that experimental data on a key nonplanar polycyclic aromatic hydrocarbon have finally become available. Amazingly, the simple additivity scheme developed by Armitage and Bird [37] successfully predicts the formation enthalpy of corannulene to within 1%.

Table 4.4: Comparison of formation enthalpy by experiments and theoretical calculations in kJ·mol^{-1} . Bold-face values are experimental.

		$C_{20}H_{10}$	C_{60}	C_{70}
$\Delta_f H°$(c)			**2355±15**[50]	
			2327±17[35]	**2555±12**[35]
			2278±14[36]	
			2422±14[25]	
		342.3±5.6[a]	**2273±15**[a]	**2369±18**[a]
$\Delta_{sub} H°$		121.4[b]	**228.7±7.3**[c]	**266.8**[d]
$\Delta_f H°$(g,exp)		**463.7**[e]	**2501±17**[e]	**2536**[e]
$\Delta_f H°$(g,calc)	6-31G*	490.4[38a]	2811.6[38b]	
	3-21G	504.2[38a]		
	STO-3G	516.3 [38a]		
	PM3	584.5[39]	3396[39]	3699[39]
	AM1	655.0[a]	4072[40]	4485[40]
	MNDO	561.8[a]	3640[41]	3954[41]
	MM2	460.7[42]	2175[43]	2438[43]
	MM3	503.5[42]	2401[44]	
	additivity	459.6[37]	2653[37]	2714[37]

[a] The present work.
[b] Estimated by empirical atom-atom potential in ref [28b] with crystal structure in ref [29].
[c] Determined by Diogo *et al.* (ref [36]) with some experimental values cited therein.
[d] Assumed to be (70/60)·$\Delta_{sub} H°(C_{60})$.
[e] Used the values of $\Delta_f H°$(c) in the fourth row of the table.

Chapter 5

Combustion Calorimetry of Coronene

5.1 Introduction

The thermodynamic properties of polycyclic benzenoid aromatic hydrocarbons (PBAHs) have been of great interest for ages to further the studies of petroleum processing, carcinogenic substances, and intersteller materials. The formation enthalpy not only provides one of those key values but bestows concrete physical meanings on the concepts aromaticity, resonance energy, etc. Here, the first combustion calorimetry of coronene (Figure 5.1), the largest PBAH ever measured, is presented. As described in the discussion of this chapter, the existence of six pericondensed carbons in coronene offers a critical test of several theoretical methods for their abilities to predict formation enthalpies for PBAHs.

The ratios of carbon and hydrogen atoms, $\frac{N_C}{N_H}$, of all the PBAHs for which the formation enthalpies have been measured are less than 2. These hydrocarbons are in the "most reactive" region of Dias's periodic table of hydrocarbons [78]. The ratio for coronene is 2 which comes down to the border line between "most reactive" and "intermediate reactive" regions. Thus coronene must be prone to incomplete combustion. The internal microheater of our combustion bomb brings into full play.

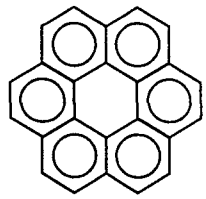

(1)

Figure 5.1: Coronene $C_{24}H_{12}$

5.2 Experimental

Sample Preparation

Two bottles of coronene sample were purchased from Tokyo Kasei Kogyo Co., Ltd. and Aldrich Chemical Co., Inc. The Aldrich's sample had been sublimed. Both samples were first analyzed by ^{1}H-NMR. Several tiny extra signals were observed around 8.2 ppm characteristic of condensed aromatic hydrocarbons (s. Figure 5.2) in both samples. Then the samples were analyzed by the reverse-phase HPLC (s. Figure 5.3(a)). As shown in the figure, three prominent peaks are observed around the retention times around 7.5, 10.5 and 14.5 min, respectively. The largest peak around 10.5 min is apparently of coronene. The other two peaks are concluded as due to impurities. If we assume the molar absorbance of impurities are as the same as that of coronene, the peak areas corresponds to about a few percent of impurities. The LC-MASS spectroscopy (liquid chromatography and mass spectroscopy in tandem) revealed that the 7.5-min peak was of the molecular weight of 276. The 14.5-min peak was not identified. Taking the NMR signals into account, one can infer the impurity of molecular weight 276 to be benzo[*ghi*]perylene (**2**) and/or dibenzo[*def,mno*]chrysene (**3**) (s. Figure 5.4 in page 57). If this is actually the case, the purchased samples are likely to have been obtained from petroleum by the rectification. Since the sublimation *in vacuo* did not reduce the impurity, the crude sample was recrystallized five times from toluene, chromatographed over silica gel, ground to powder in an agate mortar, and dried *in vacuo* at 100℃ for two hours. The ^{1}H-NMR signals of the purified coronene showed that the impurities were reduced to less than 0.3%. The chromatogram of coronene after purification is shown in Figure 5.3(b). The calorimetric

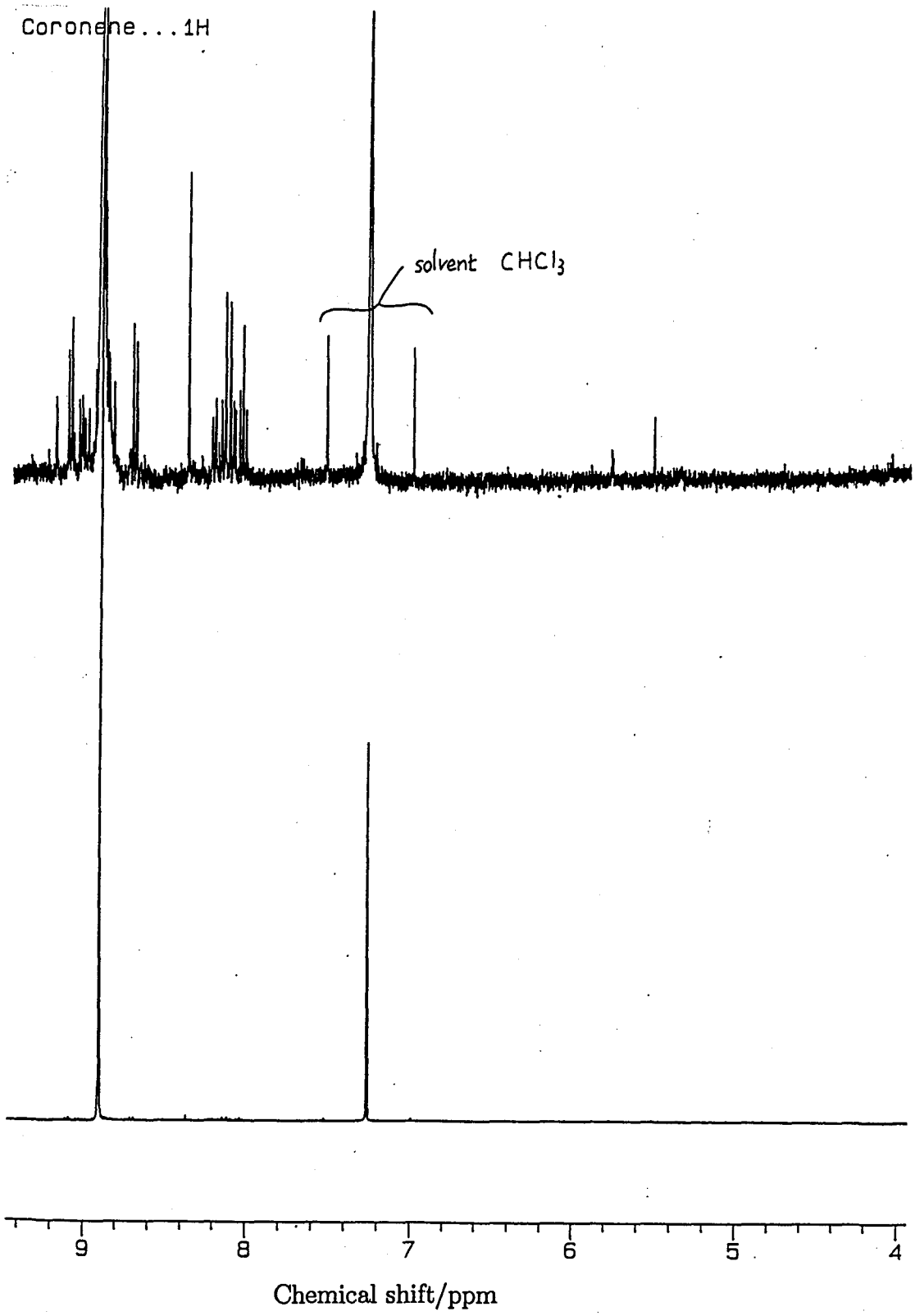

Figure 5.2: ^{1}H-NMR signals of the crude coronene sample.

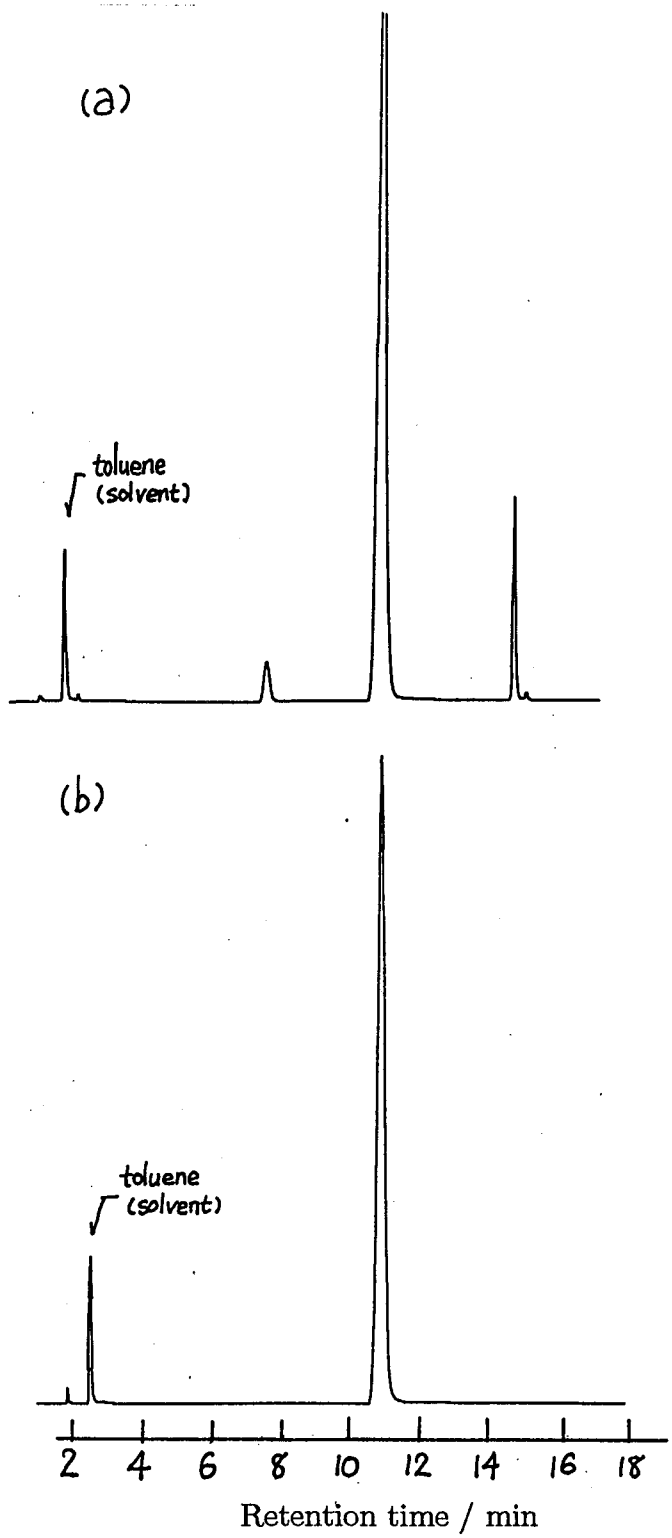

(a): before purification. (b): after purification. Column: YMC J'sphere ODS-L80 (150×46mmϕ). Eluent: CH_3CN:H_2O = 65:35. Flow rate: 2ml·min^{-1}. UV detector: 284nm.

Figure 5.3: Reverse-phase liquid chromatogram of coronene

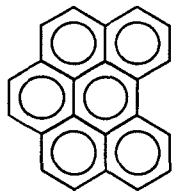

Benzo[*ghi*]perylene(**2**)

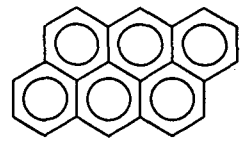

Dibenzo[*def,mno*]chrysene(**3**)

Figure 5.4: Candidates of $C_{22}H_{12}$ impurities in coronene

sample was formed into pellets with a diameter of 5mm.

Calibration of the Calorimeter

The energy equivalent of the empty calorimeter and the correction factor f for the electric energy for the internal microheater were determined by burning 20mg of thermochemical standard benzoic acid (NIST SRM 39i; $\Delta_c u_{\text{cert}} = -26434$ J·g^{-1}) under certificate conditions. The results of seven calibration runs is shown in Table 5.1. The mean and standard deviation of the observed energy equivalents ϵ° was (1372.70 ± 0.27) J·K^{-1}. The correction factor f was determined to be (1.00149 ± 0.00040).

Combustion Calorimetry of Coronene

The coronene sample was burned under an oxygen pressure of 3.04 MPa in the presence of 24 mg of water in the microbomb. The heating period for the internal microheater was 19 s. No carbon soot was detected by visual observation of the crucible. No carbon monoxide was detected from the bomb gas after combustion. The amount of nitric acid, which was formed by the oxidation of nitrogen impurity contained in the oxygen gas, was determined by UV spectrometry of the bomb solution. The contribution of enthalpies of formation and solution of the nitric acid to the calorimetry were taken into account. The density and specific heat capacity of coronene were taken to be 1.39 g·cm^{-3} from the crystal structure in ref. [52] and 1.045 J·K^{-1}g^{-1} in ref. [51], respectively. These values were used for the buoyancy correction and the reduction of the experimental results to the standard state values. The results of each combustion run are shown in Table 5.2.

Table 5.1: Results of calibration for coronene with benzoic acid

Exp. No.	1	2	3	4
m_B/mg	19.7364	19.7205	17.8051	19.6853
m(fuse)/mg	0.2302	0.1830	0.1826	0.1637
$n(HNO_3)/\mu$mol	1.226	1.011	0.928	0.652
ϵ^i/J·K^{-1}	0.357	0.357	0.355	0.357
ϵ^f/J·K^{-1}	0.380	0.380	0.375	0.380
T_i/ ℃	24.57940	24.57976	24.57963	24.57922
T_f/ ℃	25.07810	25.07646	25.04635	25.07528
ΔT_c/mK	63.12	63.26	69.72	63.78
ΔT_{ad}/mK	435.58	433.43	396.99	432.28
E_{ign}/J	0.146	0.097	0.121	0.119
E_{el}/J	65.884	65.193	65.408	65.380
$-\Delta_{IBP}U$/J	532.443	529.823	479.164	527.978
$\Delta U(HNO_3)$/J	0.073	0.060	0.055	0.039
$-m_B\Delta_c u$/J	521.309	520.889	470.297	519.960
ϵ°/J·K^{-1}	1373.59	1372.67	1371.69	1372.56

Exp. No.	5	6	7
m_B/mg	20.6351	20.3479	19.7736
m(fuse)/mg	0.1896	0.2258	0.2073
$n(HNO_3)/\mu$mol	0.928	0.802	0.950
ϵ^i/J·K^{-1}	0.358	0.358	0.357
ϵ^f/J·K^{-1}	0.382	0.381	0.380
T_i/ ℃	24.57815	24.57889	24.57898
T_f/ ℃	25.08913	25.08588	25.07677
ΔT_c/mK	59.45	60.44	62.79
ΔT_{ad}/mK	451.53	446.55	435.00
E_{ign}/J	0.130	0.161	0.086
E_{el}/J	65.525	65.021	64.583
$-\Delta_{IBP}U$/J	554.303	548.379	532.349
$\Delta U(HNO_3)$/J	0.055	0.048	0.057
$-m_B\Delta_c u$/J	545.047	537.461	522.292
ϵ°/J·K^{-1}	1372.64	1373.64	1372.09

m_B: Mass of benzoic acid. m(fuse): Mass of polyethylene fuse. $n(HNO_3)$: Amount of HNO_3 ϵ^i: Energy equivalent of the bomb contents in the initial state. ϵ^f: Energy equivalent of the bomb contents in the final state. T_i: Initial temperature of the reaction period. T_f: Final temperature of the reaction period. ΔT_c: Correction to the temperature rise. ΔT_{ad}: Adiabatic temperature rise. E_{ign}: Ignition energy. E_{el}: Electric energy to the internal microheater. IBP: Isothermal bomb process. $\Delta U(HNO_3)$: Energy change associated with the formation of HNO_3. ΔU_Σ: Standard-state correction. ϵ°: Energy equivalent of the standard calorimetric system (without the contents).

Table 5.2: Results of combustion calorimetry of coronene

Exp. No.	1	2	3	4
m(compd.)/mg	11.0401	14.8522	14.7080	13.8926
m(fuse)/mg	0.2998	0.2761	0.1762	0.2083
$n(HNO_3)/\mu$mol	1.513	0.893	0.397	0.770
ϵ^i/J·K^{-1}	0.345	0.349	0.349	0.348
ϵ^f/J·K^{-1}	0.357	0.365	0.364	0.363
T_i/ ℃	24.57993	24.58043	24.57975	24.57983
T_f/ ℃	25.01473	25.10525	25.09119	25.08074
ΔT_c/mK	77.03	57.52	60.01	62.28
ΔT_{ad}/mK	357.77	467.29	451.42	438.63
E_{ign}/J	0.084	0.153	0.096	0.134
E_{el}/J	61.337	69.036	57.854	69.573
$-\Delta_{IBP} U$/J	429.810	572.428	561.870	532.550
$\Delta U(HNO_3)$/J	0.090	0.053	0.024	0.046
ΔU_Σ/J	0.282	0.389	0.383	0.360
$-\Delta_c u°$(c)/J·g^{-1}	37640.6	37651.1	37619.3	37609.9
$-\Delta_c U°$(c)/kJ·mol^{-1}	11305.7	11308.8	11299.3	11296.5

Exp. No.	5	6	7
m(compd.)/mg	12.0583	17.6734	15.2305
m(fuse)/mg	0.1752	0.2315	0.2187
$n(HNO_3)/\mu$mol	0.342	0.884	2.030
ϵ^i/J·K^{-1}	0.346	0.352	0.349
ϵ^f/J·K^{-1}	0.359	0.371	0.360
T_i/ ℃	24.57882	24.49820	24.57898
T_f/ ℃	25.06343	25.09048	25.10310
ΔT_c/mK	65.89	60.25	56.54
ΔT_{ad}/mK	418.72	532.03	467.59
E_{ign}/J	0.123	0.119	0.109
E_{el}/J	112.643	53.746	57.756
$-\Delta_{IBP} U$/J	462.152	676.636	584.161
$\Delta U(HNO_3)$/J	0.020	0.053	0.121
ΔU_Σ/J	0.308	0.471	0.399
$-\Delta_c u°$(c)/J·g^{-1}	37626.4	37649.4	37655.6
$-\Delta_c U°$(c)/kJ·mol^{-1}	11301.4	11308.3	11310.2

m(compd.): Sample mass. m(fuse): Mass of polyethylene fuse. ΔT_{ad}: Adiabatic temperature rise. E_{ign}: Ignition energy. E_{el}: Electric energy to the internal microheater. IBP: Isothermal bomb process. $\Delta_c u°$(c): Standard specific energy of combustion. $\Delta_c U°$(c): Standard molar energy of combustion.

5.3 Result and Discussion

The mean value and standard deviation of the specific energy of combustion $\Delta_c u°(c)$ was $-(37636.0 \pm 6.7)$ J·g^{-1} . The standard thermodynamic quantities of coronene are shown in Table 5.4. Reduction to standard state was carried out by following the literature procedure [3]. The values of $\Delta_c U°(c)$ and $\Delta_f H°(c)$ refer to the following reactions, respectively:

$$C_{24}H_{12}(c) + 27O_2(g) \longrightarrow 24CO_2(g) + 6H_2O(l)$$

$$24C(\text{graphite}) + 6H_2(g) \longrightarrow C_{24}H_{12}(c)$$

For calculation of $\Delta_f H°(c)$ value, the CODATA recommended standard formation enthalpy of $CO_2(g)$ $-(393.51 \pm 0.13)$ kJ·mol^{-1} and of $H_2O(g)$ $-(285.830 \pm 0.042)$ kJ·mol^{-1} were used [4]. Uncertainties are twice the final overall standard deviation of the mean according to the rule of error propagation.

In Table 5.3, several sublimation enthalpies of coronene determined experimentally and thoretically are shown. Discrepancies among them are considerable. But there is no unprejudiced way to pick out one and reject others. Thus, the average of these eight values and twice the standard deviation, (142.9 ± 6.0) kJ·mol^{-1} , was taken.

Table 5.3: Experimental and calculated sublimation enthalpies of coronene

References		$\Delta_{sub} H°$/kJ·mol^{-1}
Inokuchi [32]*		151.0
Wakayama *et al.* [34]*		128.4
Murray *et al.* [74]*		135.9 ± 3.1
Hoyer *et al.* [75]*		146.8
Boyd *et al.* [76]†	I	149.8
	II	139.7
	III	138.9
	IV	152.3

*Experimental. †Calculation.

In Table 5.5, the present value of $\Delta_f H°$(coronene,g) is compared with those predicted theoretically. Clearly, additivity methods without explicit consideration of resonance energy (A, C and D) fail to predict the formation enthalpy correctly. Although these three

Table 5.4: Standard thermodynamic quantities of coronene at 298.15K.

$\Delta_c u°(c)/J{\cdot}g^{-1}$	-37636 ± 20
$\Delta_c U°(c)/kJ{\cdot}mol^{-1}$	-11304.3 ± 6.1
$\Delta_c H°(c)/kJ{\cdot}mol^{-1}$	-11311.7 ± 6.1
$\Delta_f H°(c)/kJ{\cdot}mol^{-1}$	152.5 ± 6.9
$\Delta_{sub} H°/kJ{\cdot}mol^{-1}$	142.9 ± 6.0
$\Delta_f H°(g)/kJ{\cdot}mol^{-1}$	295.4 ± 9.1

methods have been devised exclusively for PBAHs and fairly successful in predicting the formation enthalpies of catacondensed PBAHs, they all predict that coronene be less stable than actually is. This implies that the pericondensation brings more stabilization than the additivity of resonance energy is supposed and consequently that the resonance energy cannot be expressed in additive terms. This had been noticed by Stein who argued thereafter that the resonance energy of PBAH depends on its peripheral topology [53]. The Dorofeeva's simple group additivity scheme E is seemingly successful. However, the fatal flaw of this method is that this scheme gives -2.710 kJ·mol^{-1} for the formation enthalpy of a single graphite sheet. This value is unacceptable: it should be a positive quantity. Disch's *ab initio*/group equivalents method with large basis sets is again successful in predicting the formation enthalpy (s. Table 4.4 in Chapter 4). Although the simple additivity method is not successful, the value of Herndon's group additivity/resonance energy method (O), for which the formation enthalpy of PBAH is expressed as a sum of additive group terms and a resonance energy term, agrees well with the present result. However, as mentioned in the next chapter, there is a flaw in the Kekulé structure count resonance energy used in the Herndon's method.

Table 5.5: $\Delta_f H°(g)$ of coronene: experimental and calculated values

		Method	$\Delta_f H°(g)/kJ \cdot mol^{-1}$
	The present work	Experimental	**295.4±9.1**
A	Cox *et al.* [80]	Bond Additivity[a]	355.6
B	Herndon *et al.* [60a]	Group Additivity+ln(SC)[a,f]	303.8
C	Somayajulu *et al.* [79]	Triatomic Additivity[a]	340.2
D	Stein *et al.* [54b]	Group Additivity	322.6
E	Dorofeeva *et al.* [77b]	Group Additivity[a]	295.7
F		STO-3G/rxn IIIa[b]	256.5
G		6-31G*/rxn IIIa[b]	288.7
H		STO-3G/rxn IIIb[b]	277.4
I	Disch *et al.* [38d]	6-31G*/rxn IIIb[b]	277.4
J		STO-3G/Group Equivalents[c]	283.7
K		6-31G*/Group Equivalents[c]	283.7
L		6-31G*/Herndon Correction[a,d]	313.1
M		Molecular Mechanics	326.9
N	Herndon *et al.* [59]	Group Additivity+ln(SC)[f] (MM)[e]	336.5
O		Group Additivity+ln(SC)[f] (exp)[a,e]	307.9

[a]The heat of formation of coronene is not shown explicitly in the literature. Calculated by the present author with the parameters given therein. [b]Derived by considering some homodesmic reactions of which reaction heats were determined by *ab initio* calculation. See ref. [38d]. [c]Group equivalents were determined by fitting the experimental heats of formation with *ab initio* molecular energies. [d]Calculated by the empirical converting function of *ab initio* total energy into the heat of formation proposed by Herndon [58]. [e]Group parameters and the coefficient of resonance energy were determined by fitting the result of molecular mechanics and experimental values, respectively. [f]Structure count resonance energy.

Chapter 6

Energetics of Polycyclic Benzenoid Aromatic Hydrocarbons (PBAHs)

6.1 Introduction

In this chapter a group additivity (GA) scheme incorporating resonance energy is proposed. GA scheme for PBAHs was originally proposed by Stein *et al.* [54] as an extension of Benson group additivity scheme [55]. They introduced four group parameters to predict the formation enthalpies, intrinsic entropies, and heat capacities of PBAHs. They assert that the resonance energy is automatically included into each parameter. However, Herndon claimed that GA scheme for PBAHs would never be successful unless the resonance energy is separately considered, because the resonance energy depends on the global structure of the molecule and is accordingly far from additive [60a, 59]. For instance, Stein's GA scheme gives the same formation enthalpies for dibenzo[*de,mn*]naphthacene (**12**) and dibenzo[*de,qr*]naphthacene (**13**), and for perylene (**9**) and benzo[*e*]pyrene (**10**). In both cases, the resonance energies are significantly different from each other.

The aim of this chapter is to show how the resonance energy can be properly incorporated into the GA scheme, i.e. the molecular energy can be separated into additive component and global component. Once GA scheme is improved in this way, the evaluated additive bond energies and resonance energy provide the reference energy not only for planar PBAHs but for non-planar hydrocarbons and carbon clusters discussed in the next chapter.

6.2 Resonance Energy of PBAH

Resonance energy, which is an important quantity on "aromaticity"*, is defined as an extra stability resulting from the π-electron delocalization due to any cyclic conjugation of the molecule†. It was more than a quater century ago that Dewar and de Llano [90] defined the resonance energy as the difference in the formation enthalpies of the actual molecule and of the hypothetical reference molecule which is composed of isolated localized single and double bonds. This Dewar type resonance energy (DRE) is derived explicitly in the unit of energy. An alternative resonance energy was proposed by Hess and Shaad [91] from the theoretical point of view. In the wake of the failure of Hückel's delocalization energy as a measure of resonance energy, Hess *et al.* classified the chemical bonds of the reference structure into eight types and attributed an empirical value to each type of bonds. The Hess-Shaad type resonance energy (HSRE) is defined as the differnece between the sum of these reference energies and the Hückel π energy of the actual molecule. HSRE is given in the unit of β (the resonance integral of Hückel method). A flaw of HSRE is that there is not always a unique reference structure of a molecule. For example, two different reference energies can be derived for naphthalene.

Although both DRE and HSRE have been successfully applied to planar molecules, they suffer from difficulty in defining an appropriate reference structure for non-planar or ionic molecules. Several analytical resonance energy schemes have been proposed in order to preclude the ambiguity in defining the reference structure and to avoid introduction of empirical parameters: Topological Resonance Energy (TRE) by Aihara [64] and Gutman *et al.* [66], Conjugate Circuit model by Randić [68], Kekulé structure count model based on the valence-bond theory by Herndon *et al.* [61], and so forth (s. ref. [92]). Among these resonance energies, TRE is mainly used throughout the following discussions. It is thus relevant to introduce here how TRE is derived.

It is known that the coefficients of the Hückel secular polynomial $P(G, x)$ can be derived with the aid of graph theory — the Sachs graph [67]. A set of Sachs graphs for a conjugated

*General discussion on the aromaticity concept is reviewed in refs. [92, 93, 94].

†A controversy on this point (i.e. "Is delocalization a driving force in chemistry?") has been raised by Hilberty *et al.* [89].

Table 6.1: Experimental $\Delta_f H°$, $\Delta_a H°$, and TRE for PBAHs

Molecule	$\Delta_f H°$ /kJ·mol^{-1}	$\Delta_a H°^d$	n_{CC}	n_{CH}	TRE /$\|\beta\|$
benzene(C_6H_6)	82.7[a]	5525.3	6	6	0.273[e]
naphthalene($C_{10}H_8$)	150.6[a]	8760.1	11	8	0.389[e]
anthracene($C_{14}H_{10}$)	221.6[a]	11991.8	16	10	0.475[e]
pyrene($C_{16}H_{10}$)	225.7[a]	13421.0	19	10	0.598[e]
naphthacene($C_{18}H_{12}$)	302.4[a]	15213.6	21	12	0.553[e]
coronene($C_{24}H_{12}$)	295.4[b]	19520.6	30	12	0.947[e]
graphite sheet (per atom)	6.1[c]	710.6	1.5	0	0.0468[f]

[a]Ref.[23]. [b]Chapter 5. [c]Ref.[95, 96]. As the formation enthalpy of bulk graphite is defined as zero, this value corresponds to the sublimation enthalpy of infinite graphite sheet. [d]For calculation of $\Delta_a H°$, CODATA recommended values of $\Delta_f H°$(C,g) and $\Delta_f H°$(H,g) were used [4]. [e]Ref.[64d] [f]Ref.[62a]

molecule can be devided into two groups: the first group comprises the "circuits" — cyclic graphs, the second group comprises all the other graphs. If both groups are considered, the Hückel secular polynomial $P(G,x)$ is obtained. Whereas if only the second group is taken into account, another polynomial $R(G,x)$ is obtained. The meaning of $R(G,x)$ is unambiguous only for a monocyclic molecule. But Aihara and Gutman argued that $R(G,x)$ corresponds to the Hückel secular polynomial of such a molecule as is obtained if there were no cyclic conjugation while its topology is being kept. Let $\{x_1, x_2, \ldots, x_n\}$ and $\{x_1^R, x_2^R, \ldots, x_n^R\}$ be the roots of $P(G,x) = 0$ and $R(G,x) = 0$, respectively. Thus TRE is given by

$$TRE/|\beta| = \sum_{i}^{\text{occupied}} (x_i - x_i^R). \tag{6.1}$$

TRE is independent of the geometry of the molecule such as planar or non-planar but depends only on its topology. Once the topology of a molecule is given, the definition of equation (6.1) gives a unique value.

6.3 Additivity Scheme with Resonance Energy

In order to construct the GA scheme for PBAH, experimentally determined atomization enthalpies of seven molecules were used (Table 6.1): benzene(4), naphthalene(5),

benzene(**4**)

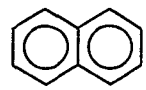

naphthalene(**5**)

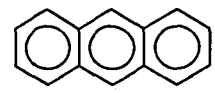

anthracene(**6**)

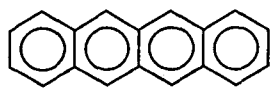

naphthacene(**7**)

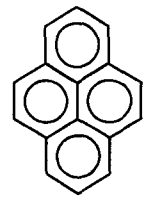

pyrene(**8**)

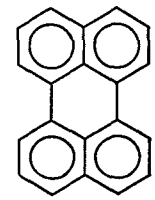

perylene(**9**)

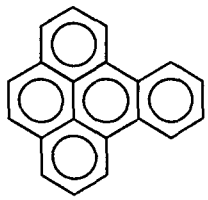

benzo[*e*]pyrene(**10**)

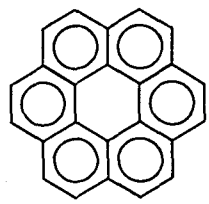

coronene(**11**)

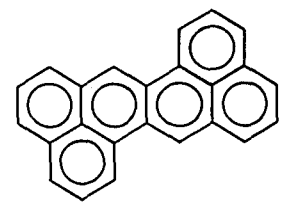

dibenzo[*de,mn*]naphthacene(**12**)

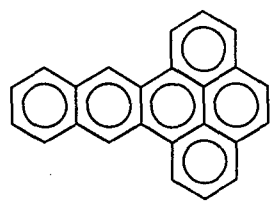

dibenzo[*de,qr*]naphthacene(**13**)

anthracene(**6**), naphthacene(**7**), pyrene(**8**), coronene(**11**) and infinite graphite sheet‡. Table 6.1 also shows the numbers of CC bonds n_{CC} and CH bonds n_{CH}, and TREs. The atomization enthalpies of these molecules were fitted by the multiple regression analysis to the three-parameter function given in the equation (6.2).

$$\Delta_a H^\circ = n_{CC}E_{CC} + n_{CH}E_{CH} + TRE\beta \tag{6.2}$$

Molecules which have hydrogen-hydrogen repulsions, such as perylene(**9**), were excluded from the present analysis. In fact, perylene is not a planar molecule because of the hydrogen-hydrogen repulsion [82, 83]. This steric term, which is not taken into account in the present study, should be considered separately [60a, 59].

Notice that the present bond type GA scheme is readily transformed to an atom type scheme by the equation

$$E(\mathrm{A}) = E_{CC} + E_{CH}$$
$$E(\mathrm{B}) = E(\mathrm{C}) = \frac{3}{2}E_{CC}$$

where group A is of a center to which one hydrogen and two peripheral carbons are bound, group B is of a center to which two A-type and one interior carbons are bound, and group C is of a center to which two B-type and one interior carbons are bound (see below).

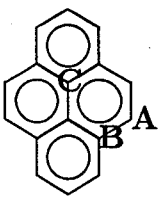

The ignored difference between E(B) and E(C) is retrieved by the consideration of resonance energy.

6.4 Evaluation and Discussion

The result of the analysis is shown in Table 6.2. In spite of the only three adjustable parameters, the GA scheme predicts the atomization enthalpies excellently well. Considering

‡Strictly speaking, graphite is not hydrocarbon. It is considered as an infinitely large PBAH.

Table 6.2: Experimental $\Delta_a H°$(expt) and GA predicted $\Delta_a H°$(GA) for PBAHs in kJ·mol^{-1}

Molecule	$\Delta_a H°$(expt)	$\Delta_a H°$(GA)	$\Delta_a H°$(expt) $-\Delta_a H°$(GA)
benzene	5525.3	5524.1	+1.2
naphthalene	8760.1	8762.3	−2.2
anthracene	11991.8	11989.7	+2.1
pyrene	13421.0	13422.0	−1.0
naphthacene	15213.6	15214.1	−0.5
coronene	19520.6	19520.2	+0.4
graphite sheet	710.6	710.8	−0.2

E_{CC} = 462.6 kJ·mol^{-1} , E_{CH} = 441.6 kJ·mol^{-1} , β = 362.2 kJ·mol^{-1} ,
Standard error = 1.8 kJ·mol^{-1}

the experimental error, it could not be better. Since the difference between the formation enthalpy and atomization enthalpy is (constant)×(constant dependent on the molecule), the GA scheme based on the formation enthalpy gives the same deviation from the experimental values. While Herndon used Kekulé structure count resonance energy in his scheme [59], it was not used in the present analysis because, as Stein pointed out, different procedures of extrapolation of structure count resonance energy to infinite size lead to different resonance enregies for graphite [53b]. In addition, whereas the multiple regression analysis for the first six molecules with TRE gives a stndard error of 2.0 kJ·mol^{-1} , a similar analysis using the structure count resonance energy gives a larger standard error of 3.1 kJ·mol^{-1} .

The resultant additive CC bond energy, 462.6 kJ·mol^{-1} , includes *localized* π-bond energy as well as σ-bond energy. In the graphite limit, it corresponds to $(2E_{C-C}+E_{C=C})/3$, where E_{C-C} and $E_{C=C}$ are the reference energies of a single bond and a double bond in Dewar's resonance theory. Letting E_{C-C}/kJ·mol^{-1} = 419.7 and $E_{C=C}$/kJ·mol^{-1} = 534.3 [90c], one gets

$$\frac{2E_{C-C}+E_{C=C}}{3} = 457.9\text{kJ·mol}^{-1}$$

which is close to the present CC bond energy. The present value of Hückel resonance integral, $|\beta|$/kJ·mol^{-1} = 362.2, is also close to 343.5 kJ·mol^{-1} , which was proposed by

Table 6.3: Contributions of resonance energy to the atomization enthalpy and predicted formation enthalpies in kJ·mol^{-1}

Molecule	$\Delta_a H°$(GA)	E_π(resonance)*	$\frac{E_\pi(\text{resonance})}{n_C}$	$\Delta_f H°$(GA)
benzene	5524.1	98.9(1.79)	16.5	83.9
naphthalene	8762.3	140.9(1.61)	14.1	148.4
anthracene	11989.7	172.1(1.44)	12.3	223.7
pyrene	13422.0	216.6(1.61)	13.5	224.7
naphthacene	15214.1	200.3(1.32)	11.1	301.9
coronene	19520.2	343.0(1.76)	14.3	295.8
graphite	710.8	16.9(2.38)	16.9	5.84

*Parenthesized value is the contribution of the resonance energy to the atiomization energy, i.e. $100 \times \frac{E_\pi(\text{resonance})}{\Delta_a H°(\text{GA})}$.

Aihara [64d]. These correspondences advocate the validity of the present model.

As shown in Table 6.3, though the resonance energy plays a crucial role in the stability of PBAH, its contribution to the atomization energy is less than a few percent.

In the next chapter, it is postulated that the present CC and CH bond energies and the value of resonance integral are transferable to the general sp^2-carbon clusters and that the formation enthalpy of a single graphite sheet is to be 5.84 kJ·mol^{-1} (s. Table 6.3).

Chapter 7

Energetics of Carbon Clusters

7.1 Introduction

When Ōsawa proposed a soccerball structure as a three-dimensional aromatic molecule, everyone thought it was nothing but fanciful [84]. We had to waited up until Kroto *et al.* discovered the fullerenes [85] and Krätschmer *et al.* improved the practical synthesis [86]. However indeed, the fullerenes have been waiting for us for more than an aeon ever since a meteorite smashed into the Earth [87, 88]. The fact that the fullerenes have endured for a geological period makes us envisage the fullerenes are as highly stable as graphite which is the most stable phase of carbon at the ambient temperature and pressure. One of the reasons for this stability has something to do with the term "aromatic stabilization". For example, because C_{60} molecule is an assembly of twenty hexagons and twelve pentagons without periphery, the number of Kekulé structure, which can be considered as a measure of π-electron delocalization, is 12500 [120],[121]. The significant magnetic shieldings measured by ^{3}He NMR in ^{3}He@C_{60} and ^{3}He@C_{70} also imply the existence of aromatic (diamagnetic) ring current in the fullerenes [104]. Still, if the term "stable" were what fullerenes are all about, they would be merely inert "soot" because they are unable against substitution reactions which are characteristic of aromatic molecules with peripheral hydrogens. Contrary to these initial expectations, fullerenes have been found to undergo a wide variety of chemical reactions [97, 98a, 101a, 103], though many of them are not characteristic features of aromatics but of alkenes. Another prominent feature of fullerenes is that the atomic arrangement inherently has curvature which engenders the strain in the molecule. Aromaticity and strain can be two independent concepts. Fullerenes thus can

be viewed as strained aromatic molecules.

In this chapter, energetics of carbon clusters is explored in terms of the resonance energy and strain energy. A discussion on the reactivity of fullerenes is addressed in terms of the strain energy. Relative stabilities among fullerenes, fullerene onions and graphite fragments are discussed.

7.2 Haddon's POAV Analysis

In planar conjugate molecules, the π-orbitals are defined as orbitals that are *globally* orthogonal to the σ-orbitals. The term "globally" means that a π-orbital $|\pi\rangle$ on any atom i is orthogonal to a σ-orbital $|\sigma\rangle$ on any atom j, i.e.

$$\langle \pi_i | \sigma_j \rangle = 0 \quad \text{for any} \quad i, j$$

which is followed by the existance of the mirror plane on the molecule. In the case of non-planar molecules, the above $\sigma - \pi$ separability is no longer satisfied. Still, Haddon pointed out that, by relaxing the definition of separability, it is physically meaningful to define the "π-orbital" that is *locally* orthogonal to the "σ-orbitals", i.e.,

$$\langle \pi_i | \sigma_i \rangle = 0$$

but

$$\langle \pi_i | \sigma_j \rangle \neq 0 \quad \text{if} \quad i \neq j.$$

The π-orbital axis vector (POAV) is defined as such a vector that lies along the p-like-orbital which composes this π-orbital. Under the assumption that σ-orbitals lie along the each internuclear axis, the POAV is defined uniquely when the geometry of a molcule is given. Although only the direction of the POAV is used in the present study, its length also has particular meanings (s. [57]).

Let the angle between the π-orbital, which is defined in the POAV analysis, and the σ-orbital be $\theta_{\sigma\pi}$. There are three independent such angles on each atom. However, for many cases including fullerenes, these three angles are nearly equal [57a], so that we can approximately attribute a single $\theta_{\sigma\pi}$ to each atom. This $\theta_{\sigma\pi}$ provides a versatile measure of non-planarity of carbon network.

7.3 Strain and Resonance Energies of Fullerene

7.3.1 Curvature and Strain of Fullerene

Schmalz *et al.* proposed an important quantity for the curvature of fullerene cage [71]: provided that $(\theta_{\sigma\pi} - \pi/2)$ is small, for spherical, spheroidal and ellipsoidal fullerenes C_n,

$$\sum^{n}(\theta_{\sigma\pi} - \frac{\pi}{2})^2 \approx \frac{4\pi}{3\sqrt{3}} = 2.418 \tag{7.1}$$

where $\theta_{\sigma\pi}$ is given in radians. The curvature integrated over the surface of a fullerene cage is thus independent of the size of the molecule as long as $(\theta_{\sigma\pi} - \pi/2)$ is small. Equation (7.1) can be called as "curvature conservation law". As the equation (7.1) is deduced purely mathematically, this can be readily extended to a cage of genus g ($g = 0$ for sphere, $g = 1$ for donut like torus, $g = 2$ for two-hole donut, etc.),

$$\sum^{n}(\theta_{\sigma\pi} - \frac{\pi}{2})^2 \approx \frac{4\pi(g+1)}{3\sqrt{3}} = 2.418(g+1). \tag{7.2}$$

As far as a fullerene that meets the isolated pentagon rule (IPR) and is not far from a sphere in the shape is concerned, equation (7.1) is well satisfied [56, 71, 70].

In the present study, E(strain) is defined as the strain energy of a localized reference structure (*vide infra*). One can thus anticipate that E(strain) will be described by a simple force-constant model. Here we postulate that E(strain) is equal to the sum of contributions from out-of-plane deformation described by the POAV angles and from in-plane deformation described by the bond angles between σ-bonds. Thus,

$$E(\text{strain}) = \frac{1}{2}k_\theta \sum_{\text{atom}}(\theta_{\sigma\pi} - \frac{\pi}{2})^2 + \frac{1}{2}k_\phi \sum_{\text{angle}} rr'(\phi - \phi_0)^2 \tag{7.3}$$

where k_θ and k_ϕ are the force constants for the POAV angle and σ-bond angle, respectively, r and r' are the bond lengths that form the angle ϕ, and ϕ_0 is the ideal sp^2 bond angle, i.e. 120°. The term rr' is included in the in-plane deformation term of equation (7.3) in order for the force field to accord with the force-constant model proposed by Cyvin *et al.* [81].

For any spherical fullerenes, we can approximate that $\phi_{\text{hexagon}} = 120°$ and $\phi_{\text{pentagon}} = 108°$. Hence, only pentagons contribute to the second term of equation (7.3). Besides, if the bond lengths of pentagon are assumed to be constant for any spherical fullerene, since the

number of pentagon is always twelve by virtue of the Euler's theorem, the second term of equation (7.3) should be a constant independent of the size of the molecule. Consequently, substitution of the equation (7.1) into (7.3) yields

$$\begin{aligned} E(\text{strain}) &= \frac{1}{2}k_\theta \times 2.418 + \frac{1}{2}k_\phi \times 12 \times 5 \times 1.432^2 \left(\frac{\pi}{180^\circ}(120^\circ - 108^\circ)\right)^2 \\ &= \frac{1}{2}k_\theta \times 2.418 + \frac{1}{2}k_\phi \times 5.397 \quad \text{for any spherical fullerenes} \end{aligned} \tag{7.4}$$

where k_θ and k_ϕ are expressed in kJ·mol^{-1} ·rad^{-2} and kJ·mol^{-1} ·rad^{-2} · Å^{-2}, respectively, and bond length of a pentagon is taken to be 1.432Å which is the value in C_{60} [101b]. Therefore, we can anticipate E(strain) of a spherical fullerene is independent of its size.

7.3.2 Resonance Energy Diminution

The curvature of the conjugate molecules brings about the misalignment in the overlap region between neighboring π-orbitals and consequently diminish the Hückel resonance integral from the planar case by the factor:

$$(\text{resonance integral diminution}) \approx 1 - c(\theta_{\sigma\pi} - \frac{\pi}{2})^2 \tag{7.5}$$

where c is a positive constant and of the order of unity [57f, 57g, 72, 73]. Taking the constant c to be unity, we get the average resonance energy diminution factor γ for a non-planar molecule as

$$\gamma = \frac{1}{n}\sum^{n}\left(1 - c(\theta_{\sigma\pi} - \frac{\pi}{2})^2\right). \tag{7.6}$$

Hence, the actual resonance energy for which the topological resonance energy is TRE is

$$E_\pi(\text{resonance}) = \gamma TRE \tag{7.7}$$

In particular, substituting the equation (7.1) into (7.6), and putting $c = 1$, one gets γ for a spherical fullerene C_n as

$$\begin{aligned} \gamma &= 1 - \frac{4\pi c}{3\sqrt{3}}\frac{1}{n} \\ &= 1 - \frac{2.418}{n}. \end{aligned} \tag{7.8}$$

7.3.3 Evaluation and Discussion

Now we have the atomization enthalpy of C_{60} and C_{70} (Chapter 3) as well as of corannulene (Cahpter 4) together with additive reference bond energies (Chapter 6), and the unit value of Hückel resonance integral (Chapter 6). TREs of C_{60} and C_{70} have been obtained by Aihara *et al.* [63] and Babić *et al.* [65], respectively, in the unit of β. The present formalism of energetics integrates these terms into the expression of standard atomization enthalpy as

$$\Delta_a H^\circ = n_{CC}E_{CC} + n_{CH}E_{CH} + E_\pi(\text{resonance}) - E(\text{strain}). \tag{7.9}$$

Substituting each value into the left-hand side and the first three terms of right-hand side of equation (7.9), we can evaluate E(strain). The results are summarized in Table 7.1.

Table 7.1: Resonance and strain energies, etc of corannulene ($C_{20}H_{10}$), C_{60} and C_{70}

	$C_{20}H_{10}$	C_{60}	C_{70}
n_{CC}	25	90	105
n_{CH}	10	0	0
$\Delta_f H^\circ$(g)/kJ·mol^{-1}	463.7[a]	2501[b]	2536[b]
$\Delta_a H^\circ$(g)/kJ·mol^{-1} [c]	16049.7	40498	47531
$n_{CC}E_{CC} + n_{CH}E_{CH}$[d]	15980.9	41634	48572
E_π(resonance)-E(strain)[e]/kJ·mol^{-1}	68.8	−1136	−1042
TRE/$\lvert\beta\rvert$	0.735[f]	1.643[f]	2.036[g]
$\Sigma(\theta_{\sigma\pi} - \pi/2)^2$	0.133[h]	2.418[i]	
γ[j]	0.994	0.960	0.965
E_π(resonance)[k]/$\lvert\beta\rvert$	0.730	1.577	1.965
/kJ·mol^{-1} [l]	264.5	571	712
E(strain)/kJ·mol^{-1}	195.7	1707	1754

[a]Chapter 4. [b]Table 4.4 of Chapter 4. [c]For calculation of $\Delta_a H^\circ$, CODATA recommended values of $\Delta_f H^\circ$(C,g) and $\Delta_f H^\circ$(H,g) were used. [d]E_{CC}/kJ·mol^{-1} = 462.6 and E_{CH}/kJ·mol^{-1} = 441.6. See Table 6.2 of Chapter 6. [e]Which is identical to $\Delta_a H^\circ$–($n_{CC}E_{CC} + n_{CH}E_{CH}$). See eq.(7.9). [f]Ref. [63]. [g]Ref. [65]. [h]Ref. [57c]. [i]See eq.(7.1). [j]Resonance energy diminution factor eq.(7.6). [k]Eq.(7.7). [l]β/kJ·mol^{-1} = 362.2. See Chapter 6.

Table 7.1 shows that E_π(resonance) per carbon atom either for C_{60} or C_{70} is about 10 kJ·mol^{-1} which is comarable with that for naphthacene (s. Table 6.3 in Chapter 6). If the term "aromatic" connotes a molecule that has a significant positive E_π(resonance), C_{60}

and C_{70} should be called fairly aromatic. However, E(strain) is larger than E_π(resonance) making the overall stabilization energy negative (destabilized) relative to the localized referenece structure.

The strain energies for C_{60} and C_{70} are close to each other (1707 and 1754 kJ·mol^{-1} , respectively). The equation (7.4) is thus well satisfied. Schmalz *et al.* proposed the strain energy for a spherical fullerene as $\approx$ 1900 kJ·mol^{-1} [71] *. Their calculation is based on the out-of-plane force constant for ***planar*** polycyclic benzenoid hydrocarbons [81f], so that their value is not equal to but fairly close to the present value.

Force Constants of Carbon Skeleton

Let E(strain) of a spherical fullerene be 1731 kJ·mol^{-1} (= constant) which is the average of those of C_{60} and C_{70}. Bakke *et al.*[81b] proposed the force constants for in-plane bending mode (s. Figure 7.1) as

$$\begin{aligned} k_\phi(a) &= 241 \text{ kJ·mol}^{-1} \cdot \text{rad}^{-2} \cdot \text{Å}^{-2} \\ k_\phi(b) &= 422 \text{ kJ·mol}^{-1} \cdot \text{rad}^{-2} \cdot \text{Å}^{-2} \\ k_\phi(c) &= 211 \text{ kJ·mol}^{-1} \cdot \text{rad}^{-2} \cdot \text{Å}^{-2}. \end{aligned} \tag{7.10}$$

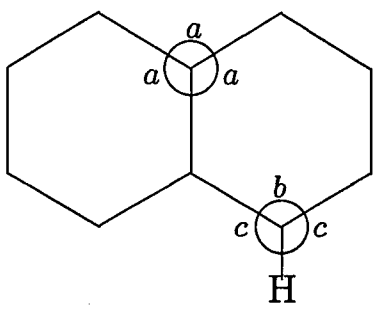

Figure 7.1: Cyvin's in-plane force constants (s. eq.(7.10))

*They did not separate the resonance energy diminution from their strain energy $\approx$ 1927 kJ·mol^{-1}. If the resonance energy diminution of the present model is taken into account, we get E(strain)$\approx$ 1900 kJ·mol^{-1}.

Substituting $k_\phi(a)$ into the equation (7.4) and solving for k_θ, we find

$$k_\theta = 893 \text{ kJ·mol}^{-1}\text{rad}^{-2}. \tag{7.11}$$

Then, in turn, substituting equation (7.10), (7.11), the molecular structure data of corannulene (s. Figure 7.2) and $\Sigma(\theta_{\sigma\pi} - \pi/2)^2 = 0.133$ (s. Table 7.1) into the equation (7.3), we get the strain energy of corannulene as 190.2 kJ·mol^{-1} which agrees well with the E(strain) = 195.7 kJ·mol^{-1} (s. Table 7.1). The validity of the present force-constant model, equation (7.3) is thus supported by another analysis.

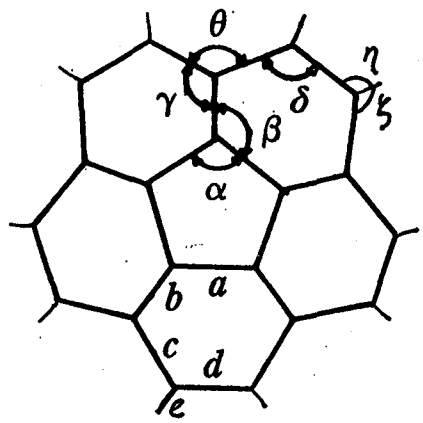

$\alpha = 108°, \beta = 123°, \gamma = 114°, \delta = 122°, \varepsilon = 130.1°, \zeta = 118°, \eta = 120°, a = 1.413$ Å$, b = 1.391$ Å$, c = 1.440$ Å$, d = 1.402$ Å$, e = 1.01$ Å

Figure 7.2: Molecular structure of corannulene (Ref. [29])

η^2-Complexation of Fullerenes

The η^2(dihapto)-complexation is one of the typical reactions for olefines such as Pt[(NC)$_2$C=C(CN)$_2$](PPh$_3$)$_2$. On the other hand, aromatic molecules rather un-

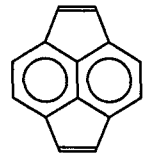

Figure 7.3: Pyracylene (Cyclopent[*fg*]acenaphthylene)

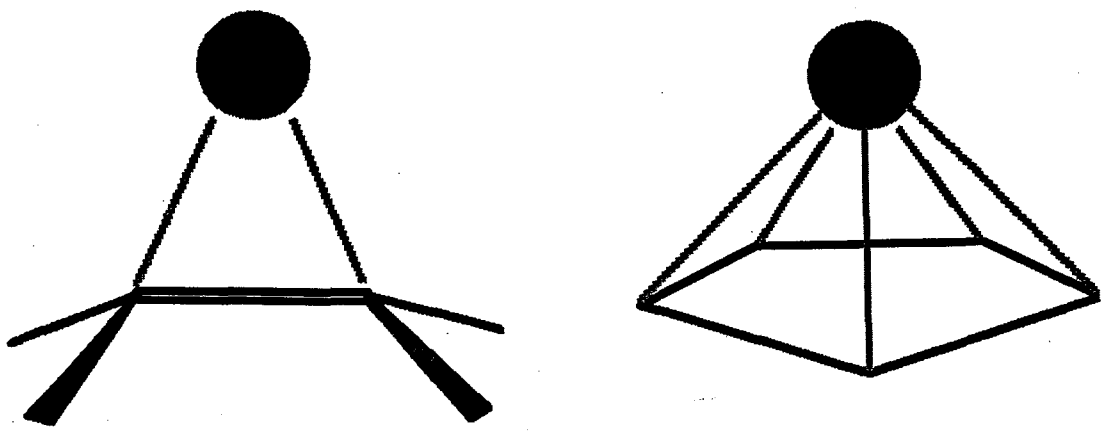

Figure 7.4: η^2- and η^5-Complexes

dergo η^5(pentahapto)- or η^6(hexahapto)-complexation than η^2-complexation, such as ferrocene = di(η^5-cyclopentadienyl)iron. Many η^2-complexes of fullerenes are known, e.g. $(Ph_3P)_2Pt(\eta^2\text{-}C_{60})$ [98b] or $(Ph)[(Ph_3P)_2(CO)(Cl)Ir(\eta^2\text{-}C_{70})$ [99] whereas neither η^5- nor η^6-complex has been known. The tendency towards η^2-complexation can be partially interpreted in terms of the strain energy. As shown in Fig 7.4, if we start from the planar molecule, the initial molecular plane is subjected to out-of-plane deformation in η^2-complexation. (Notice that all the η^2-complexes have non-planar conformations in the σ-frames even in the case of alkenes.) In the case of fullerenes, on the other hand, the carbon skeleton has the curvature in the first place. Let us take $(Ph_3P)_2Pt(\eta^2\text{-}C_{60})$ as an example. The squared POAV angle, $(\theta_{\sigma\pi} - \pi/2)^2$, of the carbon atom where Pt atom attached is 0.073 [56]. If the carbon skeleton were planar like pyracylene (Figure 7.3), the molecule would suffer an out-of-plane strain energy of about

$$2 \times \frac{1}{2} k_\theta \times 0.073 = 65 \text{ kJ·mol}^{-1}$$

in order to provide a suitable conformation for η^2-complexation. In the case of C_{60}, as $(\theta_{\sigma\pi} - \pi/2)^2 = 0.0413$ [56] in the first place, it suffers only

$$2 \times \frac{1}{2} k_\theta \times (0.073 - 0.0413) = 28 \text{ kJ·mol}^{-1}.$$

In other words, the curvature of C_{60} conceivably raise the ground state energy about 37 kJ·mol^{-1} from a hypothetical planar analog of a fullerene. This is advantageous to η^2-complexation. On the contray, the POAV angles are inclined outwards away from the axes perpendicular to either hexagon or pentagon of a fullerene, so that the overlap between π-orbitals of a fullerene and d-orbitals of a metal is poor in the η^5- or η^6-complex. Accordingly, the curvature predisposes fullerenes towards the η^2-complexation but hinders them from the η^5- or η^6-complexation.

7.4 Fullerene, Onion and Graphite

In this section, let us try to predict the formation enthalpies of larger (n $\geq$ 60) fullerenes, fullerene onions (multi-shelled fullerenes) and graphite fragments in terms of the quantities determined in the previous sections and chapters.

Graphite Fragments

Graphite fragments, which are composed of only hexagons, have inevitably dangling bonds in their peripheries. Apparently, since these dangling bonds contribute to the total energy as a destabilizing factor, the most stable graphite fragment is the one that has the least number of dangling bonds. Thus we choose the D_{6h} fragments, which has a molecular formula C_{6k^2} where k is an integer ≥ 1 and has $(9k^2-3k)$ CC bonds, as the representatives of stable graphite fragments. The resonance energies, TREs, of the D_{6h} graphite fragments of any sizes are unknown except for benzene, coronene, and graphite. As we consider relatively large fragments, let us tentatively assume that TRE per carbon atom of a graphite fragment is equal to that of graphite, i.e. $TRE(n)/n = 0.04676\beta = 16.9\text{kJ}\cdot\text{mol}^{-1}$†. The atomization enthalpy of a graphite fragment C_{6k^2} therefore can be estimated as

$$\frac{\Delta_a H^\circ(\text{graphite fragment,6k}^2)}{6k^2} = \frac{9k^2-3k}{6k^2}E_{CC} + \frac{TRE(6k^2)}{6k^2}$$

whence

$$\frac{\Delta_a H^\circ(\text{graphite fragment,n})}{n} = \left(\frac{3}{2} - \sqrt{\frac{3}{2}}\frac{1}{\sqrt{n}}\right)E_{CC} + \frac{TRE(n)}{n} \qquad (7.12)$$

where $n = 6k^2$. Substituting $E_{CC} = 462.6$ kJ·mol^{-1} and $TRE(n)/n = 16.9$ kJ·mol^{-1} into equation (7.12), one gets

$$\frac{\Delta_a H^\circ(\text{graphite fragment,n})/\text{kJ}\cdot\text{mol}^{-1}}{n} = 710.84 - \frac{566.56}{\sqrt{n}} \qquad (7.13)$$

†According to Stein *et al.*, the minimum Hess-Schaad type resonance energy (HSRE) of D_{6h} graphite fragment is in the vicinity of n=240 and its difference from infinite graphite is around 3 kJ·mol^{-1} [53a]. Though the definitions of HSRE and TRE are different, they are of the same order in magnitude. Thus in the present case, the minimum resonance enregy is probably around 14 kJ·mol^{-1} . The neglect of this resonance energy decrease, however, does not affect the present discussion seriously.

whence

$$\frac{\Delta_f H°(\text{graphite fragment,n})/\text{kJ·mol}^{-1}}{n} = \Delta_f H°(\text{C,g}) - \frac{\Delta_a H°(\text{graphite fragment,n})}{n}$$
$$= 5.84 + \frac{566.56}{\sqrt{n}}. \quad (7.14)$$

The above equation (7.14) can be applied to the piles of graphite fragments as follows. Let the number of layers be N and the number of atoms per layer be n/N. There are $(N-1)$ inter-layer interactions which correspond to the negative of the formation enthalpy of a single graphite layer, i.e. -5.84 kJ·mol^{-1} per atom (s. Table 6.3 in Chapter 6). Thence

$$\frac{\Delta_f H°(\text{N-layer,n})/\text{kJ·mol}^{-1}}{n} = \frac{N\Delta_f H°(\text{graphite fragment,n/N}) - 5.84(N-1)n/N}{n}$$
$$= 5.84\frac{1}{N} + 566.56\sqrt{\frac{N}{n}}. \quad (7.15)$$

Single-shelled Fullerenes

As long as the curvature conservation law, equation (7.1), is satisfied, we find that E(strain) $\approx$ 1731 kJ·mol^{-1} which is constant from a fullerene to another (*vide ante*). The remaining problem in the estimation of the formation enthalpies of fullerenes is thus to predict their resonance energies. Although the resonance energy depends on the topology of a molecule as a whole, the conjugate circuit model of aromatic molecules has shown that relatively small-membered circuits such as five-, six-, eight-, or ten-membered ones dominate the resonance energy [68]. As we now focus on such a fullerene as formed only by pentagons and hexagons, the number of pentagon, which contributes to anti-aromaticity, is always twelve. Moreover, as long as the IPR is satisfied, there are no eight-membered circuits which also contribute to anti-aromaticity. The number of aromatic six-membered circuits is approximately proportional to the number of carbon atoms. Thus we can confidently approximate that the resonance energy TRE of the spherical fullerene C_n is expressed as the sum of an aromatic term that is proportional to n, and a constant anti-aromatic term, i.e.

$$TRE(n) = nC_{\text{aromatic}} - C_{\text{anti-aromatic}}$$

or

$$\frac{TRE(n)}{n} = C_{\text{aromatic}} - \frac{C_{\text{anti-aromatic}}}{n}. \quad (7.16)$$

In the limit of $n \rightarrow \infty$, TRE(n)/n should coincide with that of graphite, 0.04676β. We find thus $C_{\text{aromatic}} = 0.04676\beta$. Substituting TRE(60)=$1.643\beta$ into equation (7.16), we obtain $C_{\text{anti-aromatic}} = 1.163\beta$. Similarly, with TRE(70)=2.036β, one gets $C_{\text{anti-aromatic}} = 1.237\beta$. Hence we take the average of these, $C_{\text{anti-aromatic}} = 1.20\beta$. Accordingly, the equation (7.9) is revised as

$$\begin{aligned}
\frac{\Delta_a H^\circ(\text{fullerene,n})}{n} &= \frac{3}{2}E_{CC} + \frac{\gamma TRE(n)}{n} - \frac{E(\text{strain})}{n} \\
&= \frac{3}{2}E_{CC} + \left(1 - \frac{\sum(\theta_{\sigma\pi} - \pi/2)^2}{n}\right)\left(C_{\text{aromatic}} - \frac{C_{\text{anti-aromatic}}}{n}\right) \\
&\quad - \frac{E(\text{strain})}{n} \\
&= \frac{3}{2}E_{CC} + C_{\text{aromatic}} \\
&\quad - \frac{1}{n}\left(C_{\text{anti-aromatic}} + C_{\text{aromatic}}\sum(\theta_{\sigma\pi} - \pi/2)^2 + E(\text{strain})\right) \\
&\quad + \frac{C_{\text{anti-aromatic}}\sum(\theta_{\sigma\pi} - \pi/2)^2}{n^2}. \qquad (7.17)
\end{aligned}$$

Substituting $E_{CC} = 462.6$ kJ·mol^{-1} , $C_{\text{aromatic}} = 0.04676\ \beta = 16.9$ kJ·mol^{-1} , $C_{\text{anti-aromatic}} = 1.20\ \beta = 434.7$ kJ·mol^{-1} , $\sum(\theta_{\sigma\pi} - \pi/2)^2 = 2.418$ rad^2 and $E(\text{strain}) = 1731$ kJ·mol^{-1} into equation (7.17), we get

$$\frac{\Delta_a H^\circ(\text{fullerene,n})/\text{kJ·mol}^{-1}}{n} = 710.83 - \frac{2209}{n} + \frac{1051}{n^2} \qquad (7.18)$$

whence

$$\begin{aligned}
\Delta_f H^\circ(\text{fullerene,n})/\text{kJ·mol}^{-1} &= n\Delta_f H^\circ(\text{C,g}) - \Delta_a H^\circ(\text{fullerene,n}) \\
&= 5.84n + 2209. \qquad (7.19)
\end{aligned}$$

As we focus on the fullerenes for which the IPR is satisfied, i.e. $n \geq 60$, the term proportional to n^{-2} in equation (7.18) is ignored in deriving equation (7.19). Bakowies *et al.* [70] and Adams *et al.* [106] proposed similar expressions for formation enthalpy of fullerene by fitting their results of theoretical calculation.

Multiply-shelled Fullerenes (Fullerene Onions)

For fullerene onions, the strain energy per shell is 1731 kJ·mol^{-1} , so that the total strain energy is 1731 kJ·mol^{-1} × (the number of shells). The fullerene onions are thus unfavoured

as compared with single-shelled fullerenes for a given number of carbon atoms as long as the strain energies are concerned. However, fullerene onions are stabilzed by the inter-shell interaction. It is thus expected that there is a crossing point where the inter-shell interaction prevails the strain energy and renders the fullerene onion more stable than single-shelled fullerene for a particular number of carbon atoms.

Consider a fullerene M-onion which is formed by covering the C_{60} with M shells (thus total M+1 shells). Assuming that the number of carbon atoms is proportional to its radius, we get

$$n_i = 60\left(\frac{R_i}{R_0}\right)^2$$

where the subscript i represents the i-th shell, n_i is the number of carbon atoms with radius R_i, and R_0 is the radius of C_{60} = 3.5 Å [101b, 102]. The inter-shell distance r is r=3.4 Å$\approx R_0$ which has been obtained by exerimental observation [111a, 111d, 112f] and by theoretical calculation [122]. Thus we get a simple relation

$$\begin{aligned} n_i &= 60\left(\frac{R_0 + ir}{R_0}\right)^2 \\ &\approx 60\left(\frac{R_0 + iR_0}{R_0}\right)^2 \\ &= 60(1+i)^2 \end{aligned} \tag{7.20}$$

which yields $n_i = 60, 240, 540, \ldots$ for successive shells, i.e. 1-Onion: C_{60+240}, 2-Onion: $C_{60+240+540}$, and so on. Incidentally, these numbers coincide with those for truncated icosahedra [71]‡. The formation enthalpy of M-onion is thus

$$\Delta_f H^\circ(\text{M-onion}) = \sum_{i=0}^{M} \Delta_f H^\circ(\text{fullerene},60(1+i)^2) + E_{\text{inter-shell}} \tag{7.21}$$

where $E_{\text{inter-shell}}$ represents the inter-shell interaction. The inter-shell distance r = 3.4 Å is also close to the inter-layer distance of graphite (3.35Å), so that the inter-shell interaction per carbon atom of fullerene onion can be assumed to be the negative of the formation enthalpy of graphite monolayer, i.e. -5.84 kJ·mol^{-1} in the present model (s. Table 6.3 in Chapter 6). The assumption that the inter-shell interaction is proportional to the number

‡In general, the number of vertices n for truncated icosahedra is given by a pair of integer h and k $(0 < h \geq k \geq 0)$ as $n = 20(h^2 + hk + k^2)$. Thus the equation (7.20) does not yield all the possible number of truncated icosahedra. See ref. [71].

of atoms in contact has been validated by *ab initio* calculation of a system of two concentric graphitic tubes [122]. Therefore, taking it into account that the inner-most and outer-most shells are in contact only on one side, one gets

$$\begin{aligned} E_{\text{inter-shell}} &= -\frac{1}{2}5.84 \cdot 60 - \sum_{i=1}^{M-1} 5.84 \cdot 60(1+i)^2 - \frac{1}{2}5.84 \cdot 60(1+M)^2 \\ &= -10 \cdot 5.84M(2M^2+6M+7). \end{aligned} \tag{7.22}$$

Substitution of the equation (7.19) and (7.22) into (7.21) yields

$$\Delta_f H^\circ(\text{M-onion}) = 5.84 \cdot 10(M+1)(M+2)(2M+3) + 2209(M+1) - 10 \cdot 5.84M(2M^2+6M+7)$$

or, dividing by the number of atoms per onion $n = \sum_{i=0}^{M} 60(1+i)^2 = 10(M+1)(M+2)(2M+3)$,

$$\begin{aligned} \frac{\Delta_f H^\circ(\text{M-onion})}{n} &= 5.84 + \frac{2209}{10(M+2)(2M+3)} - 5.84\frac{M(2M^2+6M+7)}{10(M+1)(M+2)(2M+3)} \\ &= 5.84\frac{3(M^2+2M+2)}{(M+1)(M+2)(2M+3)} + \frac{2209}{10(M+2)(2M+3)}. \end{aligned} \tag{7.23}$$

The Stable State of Carbon Clusters

In Figure 7.5, the formation enthalpies of graphite fragments (equation(7.15)), hollow fullerenes (equation(7.19)) and fullerene onions (equation(7.23)) are shown. Explicit numerical results for hollow fullerenes and onions are shown in Table 7.2. It can be seen that the most unstable speicies are graphite fragment. Tremendous number of carbon atoms are necessary to overcome the destabilization due to the dangling bonds by the stabilization by stacking of fragments. There is a crossing point at around $n \approx 10^3$ between hollow fullerenes and fullerene onions, i.e. for $n \geq 10^3$ fullerene onions are more stable than hollow fullerenes as long as their ground states are concerned. Bennemann *et al.* calculated the similar crossing point [109a], while Maiti *et al.* [110] and Tománek *et al.* [118] proposed the crossing points are at $n = 6000$ and $n = 660$, respectively, from their theoretical calculations.

A recent determination of combustion energy of fullerene soot revealed that the fullerene soot is as highly energized as C_{60} or C_{70} [107]. From this fact together with the Figure 7.5, it is inferred that in the generation process of fullerenes such as arc-discharge between carbon

Table 7.2: Formation enthalpies per carbon atom of hollow fullerenes and fullerene onions in $kJ \cdot mol^{-1}$

M	hollow fullerene		fullerene onion	
1	C_{300}	13.2	C_{60+240}	17.6
2	C_{840}	8.5	$C_{60+240+540}$	10.0
3	C_{1800}	7.1	$C_{60+240+540+960}$	6.6
4	C_{3300}	6.5	$C_{60+240+540+960+1500}$	4.7
5	C_{5460}	6.2	$C_{60+240+540+960+1500+2160}$	3.6

eletrodes or laser vapourization of graphite, the carbon vapour is quenched in early stage of spiral (curved) layer accretion onto the C_{60}-like embryo (s. ref. [108]). This is also in accord with the experimental observation that (a) the following harsh procedures *anneal* the carbonaceous materials towards the fullerene onions: electron irradiation of either fullerene soot or amorphous carbon [112], shock-wave treatment of carbon soot [114], carbon deposits generated by the laser decomposition of benzene [115], laser melting of carbon in a high-pressure cell [116] and thermal treatment of diamond nanoparticles [117], however, (b) the thermal treatment of fullerene soot, which could be considered as milder treatment than (a), yields imperfect fullerene onions with large inner cavity and polyhedral (not spherical) shape [112d, 112e]. One can thus conclude that the barrier for bond rearrangement is so high that the fullerene soot is entrapped in high energy state.

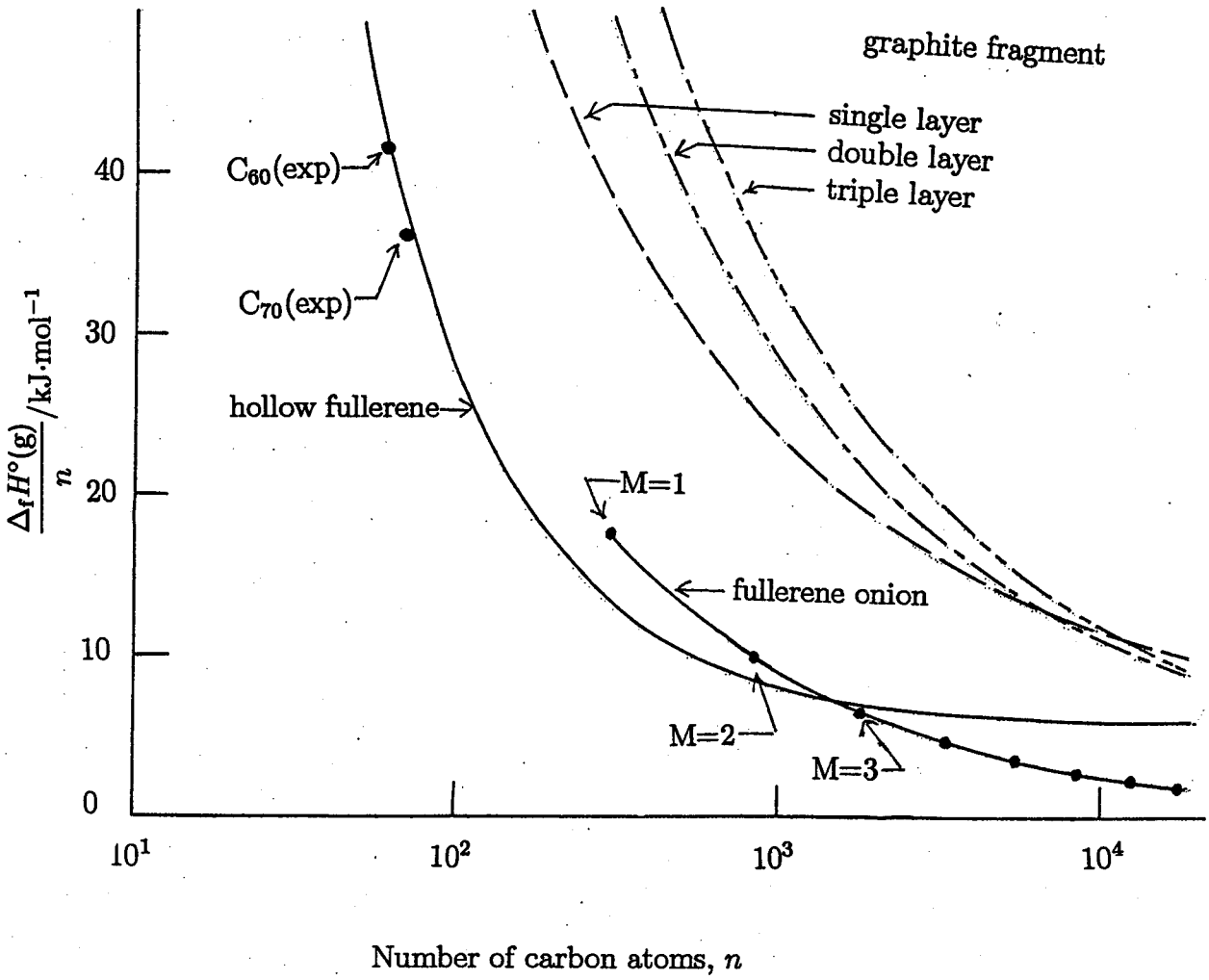

Figure 7.5: Formation enthalpies of fullerenes, onions and graphite fragments

Chapter 8

Concluding Remarks

The micro-bomb combustion calorimeter developed in the present study was found to be applicable to combustion studies using small amounts of less combustible compounds, such as fullerenes. The major innovation by which we could overcome the difficulties to reduce the sample mass was an improvement on the bomb. In particular, the microheater plays a key role in preventing the incomplete combustion. The formation enthalpies of C_{60}, C_{70}, corannulene and coronene were determined by this calorimeter. With the exception of C_{60}, they were first experimentally determined in the present study.

The atomization enthalpies of planar PBAHs were well explained as the sum of additive bond energies and topological resonance energy. It is thus concluded that the parameters determined provide a set of reference energies for other sp^2-carbon networks.

By the use of the thermodynamic quantities determined in the present study as a basis, energetics of non-planar sp^2-carbon clusters was explored. Quantitative relation among the resonance, strain and bonding energies was derived. Calculation of relative stabilities of hollow fullerenes, fullerene onions and graphite fragments revealed that the most stable forms among them are not graphite fragments but fullerene onions for an aggregate of a thousand carbon atoms. The present study will be a basis for discussions on the thermodynamic properties of nano-scale carbon particles which are in the interdisciplinary area between gas-phase cluster chemistry and bulk chemistry.

The present formalism of energetics can be extended to other form of sp^2-carbon clusters by on-going measurement of a molecule which has seven-membered ring. This future extension of energetics will be applied to graphitic tori ([111d],[123],[124]), graphitic sheets of the negative Gaussian curvature ([127],[125],[126]), and more generally, to the nano-scale

carbon aggregates.

References

[1] Lavoisier, A. L.; de LaPlace, P. S. *Mem. Acad. Sci.* **1784**, 355-408.

[2] IUPAC *"Exprimental Chemical Thermodynamics Vol.1: Combustion Calorimetry"* Sunner, S.; Månsson, M. Eds., Pergamon Press, Oxford, **1979**

[3] Rossini, F. D. *"Experimental Thermochemistry"*; Interscience Publishers; New York, **1956.**

[4] CODATA Committee on Key Values for Thermodynamics, *J. Chem. Thermodyn.* **1978**, *10*, 903-906.

[5] (a) Padoa, M.; Foresti, B. *Ber. Deutsch. Chem. Gesellschaft* **1925**, *58B*, 1339-1342.
(b) Padoa, M.; Foresti, B. *Gazz. Chim. Ital.* **1923**, *53*, 493-498.

[6] (a) Roth, W. A.; Müller, F. *Chem. Ber.* **1927**, *60*, 643-645.
(b) Roth, W. A.; Ginsberg, H.; Lassé, R. *Z. Elektrochem. Angew. Phys. Chem.* **1924**, *30*, 417-420.
(c) Roth, W. A.; Lassé, R. *Z. Elektrochem. Angew. Phys. Chem.* **1924**, *30*, 607-609.

[7] (a) Eucken, A.; Meyer, L. *Chem. Fabrik* **1928**, 177-179.
(b) Eucken, A.; Meyer, L. *Chem. Fabrik* **1928**, 195-196.
(c) Eucken, A. *Chem. Zentralbl.* **1924**, *95(I)*, 815-816.

[8] McEwan, W. S.; Anderson, C. M. *Rev. Sci. Instr.* **1955**, *26*, 280-284.

[9] Mackle, H.; O'Hare, P. A. G. *Trans. Faraday Soc.* **1963**, *59*, 2693-2701.

[10] Quitzsch, K.; Schaffernicht, H.; Geiseler, G. *Z. Phys. Chem. (Leipzig)* **1963**, *223*, 200-206.

[11] Müller, W.; Schuller, D. *Ber. Bunsenges. Phys. Chem.* **1971**, *75*, 79-81.

[12] Månsson, M. *J. Chem. Thermodyn.* **1973**, *5*, 721-732.

[13] Metzger, R. M.; Kuo, C. S.; Arafat, E. S. *J. Chem. Thermodyn.* **1983**, *15*, 841-851.

[14] Knauth, P.; Sabbah, R. *Bull. Soc. Chim. Fr.* **1990**, *127*, 329-346.

[15] (a) Philp, P. *"Thèse de Specialité en Chimie Physique"* Marseille, **1969**

(b) Sabbah, R.; Coten, M. *Thermochim. Acta* **1981**, *49*, 307-317.

(c) Sabbah, R.; Antipine, I. *J. Soc. Chim. Fr.* **1987**, *3*, 392-400.

[16] Beckhaus, H.-D.; Rüchardt, C.; Smisek, M. *Thermochim. Acta* **1984**, *79*, 149-159.

[17] Diogo, H. P.; Minas da Piedade, M. E. *J. Chem. Thermodyn.* **1995**, *27*, 197-206.

[18] (a) Sakiyama, M.; Nakano, T.; Seki, S. *Bull. Chem. Soc. Jpn.* **1975**, *48*, 1705-1708.

(b) Nishiyama, K.; Sakiyama, M.; Seki, S.; Horita, H.; Otsubo, T.; Misumi, S. *Bull. Chem. Soc. Jpn.* **1980**, *53*, 869-877.

(c) Nagano, Y.; Sakiyama, M.; Fujiwara, T.; Kondo, Y. *J. Phys. Chem.* **1988**, *92*, 5823-5827.

[19] Yamane, T.; Sakiyama, M. unpublished

[20] Parks, G. S.; Lighht, D. W. *J. Am. Chem. Soc.* **1934**, *56*, 1511-1513.

[21] Johnson, W. H.; Prosen, E. J. *J. Res. Natl. Bur. Stand. (U.S.)* **1975**, *A79*, 481-486.

[22] (a) Atake, T.; Tanaka, T.; Kawaji, H.; Kikuchi, K.; Saito, K.; Suzuki, S.; Achiba, Y.; Ikemoto, I. *Chem. Phys. Lett.* **1992**, *196*, 321-324.

(b) Kikuchi, K.; Nakahara, N.; Wakabayashi, T.; Honda, M.; Matsumiya, H.; Moriwaki, T.; Suzuki, S.; Shiromaru, H.; Saito, K.; Yamauchi, K.; Ikemoto, I.; Achiba, Y. *Chem. Phys. Lett.* **1992**, *188*, 177-180.

[23] Pedley, J. B.; Naylor, R. D.; Kirby, S. P.; *"Thermochemical Data of Organic Compounds"* 2nd ed., Chapman and Hall, London, **1986**.

[24] Beckhaus, H.; Rüchardt, C.; Kao, M.; Diederich, F.; Foote, C. S.; *Angew. Chem., Int. Ed. Engl.* **1992**, *31*, 63-64.

[25] Steele, W. V.; Chirico, R. D.; Smith, N. K.; Billups, W. E.; Elmore, P. R.; Wheeler, A. E. *J. Phys. Chem.* **1992**, *96*, 4731-4733.

[26] (a) Barth, W. E. Ph.D. Thesis, University of Michigan, **1966**.

(b) Barth, W. E.; Lawton, R G. *J. Am. Chem. Soc.* **1966**, *88*, 380-381.

(c) Barth, W. E.; Lawton, R. G. *J. Am. Chem. Soc.* **1971**, *93*, 1730-1745.

[27] (a) Scott, L. T.; Hashemi, M. M.; Meyer, D. T.; Warren, H. B. *J. Am. Chem. Soc.* **1991**, *113*, 7082-7084.

(b) Scott, L. T.; Hashemi, M. M.; Bratcher, M. S. *J. Am. Chem. Soc.* **1992**, *114*, 1920-1921.

(c) Borchardt, A.; Fuchicello, A.; Kilway, K. V.; Baldridge, K. K.; Siegel, J. S. *J. Am. Chem. Soc.* **1992**,*114*, 1921-1923.

(d) Scott. L. T.; Cheng, P.-C.; Bratcher, M. S. Abstract No. 64, *Seventh International Symposium on Novel Aromatic Compounds*, Victoria, Canada, July 19-24, **1992**.

(e) Cheng, P.-C. M.S. Thesis, University of Nevada, Reno, **1992**

[28] (a) Williams, D. E. *J. Chem. Phys.* **1967**, *47*, 4680-4684.

(b) Williams, D. E. *J. Chem. Phys.* **1966**, *45*, 3770-3778.

[29] Hanson, J. C.; Nordman, C. E. *Acta Cryst.* **1976**, *B32*, 1147-1153.

[30] Stewart, J. J. P. *QCPE Bull.* **1989**, *9*, 10-15.

[31] Takagi, T.; Matsumura, K.; Noda A.; Onozawa N.; Fujiwara, H. *Bulletin of Computation Center Osaka University* **1992**, *22*, 1.

[32] 井口 洋夫(Inokuchi, H.) 日本化學雜誌(*J. Chem. Soc. Jpn.*) **1951**, *72*, 552-555.

[33] Inokuchi, H.; Shiba, S.; Handa, T.; Akamatu, H. *Bull. Chem. Soc. Jpn.* **1952**, *25*, 299-302.

[34] Wakayama, N.; Inokuchi, H. *Bull. Chem. Soc. Jpn.* **1967**, *40*, 2267-2271.

[35] Beckhaus, H.-D.; Verevkin, S.; Rüchardt, C.; Diederich, F.; Thilgen, C.; ter Meer, H.-U.; Mohn, H.; Müller, W. *Angew. Chem., Int. Ed. Engl.* **1994**, *33*, 996-998.

[36] Diogo, H. P.; Minas da Piedade, M. E.; Dennis, T. J. S.; Hare, J. P.; Kroto, H. W.; Taylor, R.; Walton, D. R. M. *J. Chem. Soc., Faraday Trans.* **1993**, *89*, 3541-3544.

[37] Armitage, D. A.; Bird, C. W. *Tetrahedron Lett.* **1993**, *34*, 5811-5812.

[38] (a) Schulman, J. M.; Peck, R. C.; Disch, R. L. *J. Am. Chem. Soc.* **1989**, *111*, 5675-5680.

(b) Schulman, J. L.; Disch, R. L. *J. Chem. Soc. Chem. Commun.* **1991**, 411-412.

(c) Peck, R. C.; Sculman, J. M.; Disch, R. L. *J. Phys. Chem.* **1990**, *94*, 6637-6641.

(d) Disch, R. L.; Schulman, J. M.; Peck, R. C. *J. Phys. Chem.* **1992**, *96*, 3998-4002.

[39] Matsuzawa, N.; Dixon, D. A. *J. Phys. Chem.* **1992**,*96*, 6241-6247.

[40] Rudziński, J. M.; Slanina, Z.; Togasi, M.; Ōsawa, E.; Iizuka, T. *Thermochimi. Acta.* **1988**, *125*, 155-162.

[41] Newton, M. D.; Stanton, R. E. *J. Am. Chem. Soc.* **1986**, *108*, 2469-2470.

[42] Allinger, N. L.; Nevins, N.; Lii, J.-H. personal communication.

[43] Froimowitz, M. *J. Comput. Chem.* **1991**, *12*, 1129-1133.

[44] Diederich, F.; Whetten, R. L.; Thilgen, C.; Ettl, R.; Chao, I.; Alvarez, M. M. *Science* **1991**, *254*, 1768-1770.

[45] Beckers, M. *Bull. Soc. Chim. Belg.* **1931**, *40*, 518-610.

[46] Keffler, L. J. P. *J. Chim. Phys.* **1931**, *28*, 457-469.

[47] Stiehler, R. D.; Huffman, H. M. *J. Am. Chem. Soc.* **1935**, *57*, 1734-1740.

[48] Milone, M.; Rossignoli, P. *Gazz. Chim. Ital.* **1932**, *62*, 644-655.

[49] Badoche, M. *Bull. Soc. Chim. Fr.* **1937**, *4*, 549-558.

[50] Kolesov, V. P.; Pimenova, S. M.; Pavlovich, V. K.; Tamm, N. V.; Kurskaya, A. submitted to *Molecular Materials.*

[51] Wong, W.-K.; Westrum, Jr., E. F. *Mol. Cryst. Liq. Cryst.* **1980**, *61*, 207-228.

[52] Fawcett, J. K.; Trotter, J. *Proc. R. Soc. (London)* **1966**, *A289*, 366-376.

[53] (a) Stein, S. E.; Brown, R. L. *J. Am. Chem. Soc.* **1987**, *109*, 3721-3729.
(b) Stein, S. E.; Brown, R. L. *"Molecular Structures and Energetics"*; Liebman and Greenberg, Eds.; VCH Publishers, **1987**, Chapter 2.

[54] (a) Stein, S. E.; Fahr, A. *J. Phys. Chem.* **1985**, *89*, 3714-3725.
(b) Stein, S. E.; Golden, D. M.; Benson, S. W. *J. Phys. Chem.* **1977**, *81*, 314-317

[55] (a) Benson, S. W. *"Thermochemical Kinetics"*, 2nd ed.; Wiley; New York, **1976.**
(b) Benson, S. W.; Cruickshank, F. R.; Golden, D. M.; Haugen, G. R.; O'Neal, H. E.; Rodgers, A. S.; Shaw, R.; Walsh, R. *Chem. Rev.* **1969**, *69*, 279-324.

[56] Haddon, R. C. *Science* **1993**, *261*, 1545-1550.

[57] (a) Haddon, R. C. *J. Am. Chem. Soc.* **1990**, *112*, 3385-3389. [Additions and Corrections: *ibid.* **1990**, *112*, 8217.]
(b) Haddon, R. C. *Acc. Chem. Res.* **1988**, *21*, 243-249.
(c) Haddon, R. C. *J. Am. Chem. Soc.* **1987**, *109*, 1676-1685.
(d) Haddon, R. C. *J. Phys. Chem.* **1987**, *91*, 3719-3720.
(e) Haddon, R. C. *J. Am. Chem. Soc.* **1986**, *108*, 2837-2842.
(f) Haddon, R. C.; Brus, L. E.; Raghavachari, K. *Chem. Phys. Lett.* **1986**, *131*, 165-169.
(g) Haddon, R. C.; Brus, L. E.; Raghavachari, K. *Chem. Phys. Lett.* **1986**, *125*, 459-464.

[58] Herndon, W. C. *Chem. Phys. Lett.* **1995**, *234*, 82-86.

[59] Herndon, W. C.; Nowak, P. C.; Connor, D. A.; Lin. P.-P. *J. Am. Chem. Soc.* **1992**, *114*, 41-47.

[60] (a) Herndon, W. C. *Thermochimi. Acta.* **1974**, *8*, 225-237.
(b) Herndon, W. C. *Tetrahedron* **1973**, *29*, 3-12.
(c) Herndon, W. C. *J. Am. Chem. Soc.* **1973**, *95*, 2404-2406.

[61] (a) Herndon, W. C. *Israel J. Chem.* **1980**, *20*, 270-275.
(b) Herndon, W. C. *Israel J. Chem.* **1980**, *20*, 276-280.
(c) Swinborne-Sheldrake, R.; Herndon, W. C. ; Gutman, I. *Tetrahedron Lett.* **1975**, 755-758.

[62] (a) Aihara, J.; Yamabe, T.; Hosoya, H. *Synth. Met.* **1994**, *64*, 309-313.
(b) Aihara, J. *J. Phys. Chem.* **1994**, *98*, 9773-9776.

[63] Aihara, J.; Hosoya, H. *Bull. Chem. Soc. Jpn.* **1988**, *61*, 2657-2659.

[64] (a) Aihara, J. *J. Am. Chem. Soc.* **1976**, *98*, 2750-2758.
(b) 相原　惇一 (Aihara, J.), 熱測定 (*Netsu Sokutei*) **1985**, *12*, 61-72.
(c) 相原　惇一 (Aihara, J.), 化学の領域 (*Kagaku no Ryōiki*) **1976**, *30*, 269-278.
(d) 相原　惇一 (Aihara, J.), 化学の領域 (*Kagaku no Ryōiki*) **1976**, *30*, 379-391.
(e) 相原　惇一 (Aihara, J.), 化学の領域 (*Kagaku no Ryōiki*) **1976**, *30*, 812-821.

[65] Babić, D.; Ori, O. *Chem. Phys. Lett.* **1995**, *234*, 240-244.

[66] Gutman, I.; Milun, M.; Trinajstić, N. *J. Am. Chem. Soc.* **1977**. *99*, 1692-1704.

[67] (a) 飛田　満彦 "有機量子化学入門" 学会出版センター, **1981**, 第４章.
(b) Graovac, A.; Gutman, I.; Trinajstić, N. *"Topological Approach to the Chemistry of Conjugated Molecules"* Springer Verlag, **1977**.

[68] (a) Klein, D. J.; Trinajstić, N. *Pure Appl. Chem.* **1989**, *61*, 2107-2115.
(b) Randić, M.; Plavšić, D.; Trinajstić, N. *J. Molec. Struc.* **1989**, *185*, 249-274.
(c) Randić, M. *Chem. Phys. Lett.* **1976**, *38*, 68-70.
(d) Randić, M. *J. Am. Chem. Soc.* **1977**, *99*, 444-450.

[69] Randić, M.; Trinajstić, N. *J. Am. Chem. Soc.* **1987**, *109*, 6923-6926.

[70] Bakowies, D.; Thiel, W. *J. Am. Chem. Soc.* **1991**, *113*, 3704-3714.

[71] Schmalz, T. G.; Seitz, W. A.; Klein, D. J.; Hite, G. E. *J. Am. Chem. Soc.* **1988**, *110*, 1113-1127.

[72] Klein, D. J.; Schmalz, T. G.; Seitz, W. A.; Hite, G. E. *J. Am. Chem. Soc.* **1986**, *108*, 1301-1302.

[73] Fowler, P. W.; Woolrich, J. *Chem. Phys. Lett.* **1986**, *127*, 78-83.

[74] Murray, J. J.; Pottie, R. F. *Can. J. Chem.* **1974**, *52*, 557-563.

[75] Hoyer, H.; Peperle, W. *Z. Elktrochem., Ber. Bunsenges. Phys. Chem.* **1958**, *62*, 61-66.

[76] Boyd, R. K.; Fyfe, C. A.; Wright, D. A. *J. Phys. Chem. Solids* **1974**, *35*, 1355-1365.

[77] (a) Moiseeva, N. F.; Dorofeeva, O. V.; Jorish, V. S. *Thermochim. Acta* **1990**, *168*, 179-186.

(b) Moiseeva, N. F.; Dorofeeva, O. V. *Thermochim. Acta* **1989**, *153*, 77-85.

(c) Dorofeeva, O. V.; Gurvich, L. V.; Cyvin, S. J. *Thermochim. Acta* **1986**, *102*, 59-66.

[78] Dias, J. R. *Acc. Chem. Res.* **1985**, *18*, 241-248.

[79] Somayajulu, G. R.; Zwolinski, B. J. *J. Chem. Soc., Faraday Trans. 2* **1974**, *70*, 1928-1941.

[80] Cox, J. D.; Pilcher, G. *"Thermochemistry of Organic and Organometalic Compounds"* Academic Press, New York, N.Y., **1970**

[81] (a) Whitmer, J. C.; Cyvin, S. J.; Cyvin, B. N. *Z. Naturforsch.* **1978**, *33a*, 45-54.

(b) Bakke, A.; Cyvin, B. N.; Whitmer, J. C.; Cyvin, S. J.; Gustavsen, J. E.; Klaeboe, P. *Z. Naturforsch.* **1979**, *34a*, 579-584.

(c) Cyvin, S. J.; Cyvin, B. N.; Brunvoll, J.; Whitmer, J. C.; Klaeboe, P.; Gustavsen, J. E. *Z. Naturforsch.* **1979**, *34a*, 876-886.

(d) Cyvin, S. J.; Cyvin, B. N.; Brunvoll, J. *Z. Naturforsch.* **1979**, *34a*, 887-891.

(e) Cyvin, S. J.; Brunvoll, J.; Cyvin, B. N.; Mastryukov, V. S. *Z. Naturforsch.* **1979**, *34a*, 1512-1517.

(f) Cyvin, B. N.; Neerland, G.; Brunvoll, J.; Cyvin, S. J. *Z. Naturforsch.* **1980**, *35a*, 731-738.

[82] Tanaka, J. *Bull. Chem. Soc. Jpn.* **1963**, *36*, 1237-1249.

[83] Camerman, A.; Trotter, J. *Proc. R. Soc. (London)* **1964**, *A279*, 129-146.

[84] (a) 大澤 映二(Ōsawa, E.) 化学(*Kagaku*) **1970**, *25*, 854-563.

(b) 吉田 善一(Yoshida, Z.); 大澤 映二(Ōsawa, E.) *"芳香族性 (Aromaticity)"*; 化学同人 (Kagakudojin); 京都 (Kyoto), **1971**.

[85] Kroto, H. W.; Heath, J. R.; O'Brien, S. C.; Curl, R. F.; Smalley, R. E. *Nature* **1985**, *318*, 162-163.

[86] Krätschmer, W.; Lamb, L. D.; Fostiropoulos, D.; Huffman, R. *Nature* **1990**, *347*, 354-358.

[87] Becker, L.; Bada, J. L.; Winans, R. E.; Hunt, J. E.; Bunch, T. E.; French, B. M. *Science* **1994**, *265*, 642-645.

[88] Heymann, D.; Felipe Chibante, L. P.; Brooks, R. R.; Wolbach, W. S.; Smalley, R. E. *Science* **1994**, *265*, 645-647.

[89] (a) Hilberty, P. C.; Ohanessian, G.; Shaik, S. S. ; Flament, J. P. *Pure Appl. Chem.* **1993**, *65*, 35-45.

(b) Aihara, J. *Bull. Chem. Soc. Jpn.* **1990**, *63*, 1956-1960.

(c) Ohanessian, G.; Hilberty, P. C.; Lefour, J. M.; Flament, J. P.; Shaik, S. S. *Inorg. Chem.* **1988**, *27*, 2219-2224.

(d) Shaik, S. S.; Hilberty, J. P.; Lefour, J. M.; Ohanessian, G. *J. Am. Chem. Soc.* **1987**, *109*, 363-374.

(e) Kuwajima, S.; Soos, Z. G. *J. Am. Chem. Soc.* **1987**, *109*, 107-113.

(f) Baird, N. C. *J. Org. Chem.* **1986**, *51*, 3907-3908.

(g) Hilberty, P. C.; Shaik, S. S.; Ohanessian, G. *J. Org. Chem.* **1986**, *51*, 3908-3909.

(h) Cooper, D. L.; Gerratt, J.; Raimondi, M. *Nature* **1986**, *323*, 699-701.

(i) Hilberty, P. C.; Shaik, S. S.; Lefour, J. M.; Ohanessian, G. *J. Org. Chem.* **1985**, *50*, 4657-4659.

[90] (a) Dewar, M. J. S.; Gleicher, G. J. *J. Am. Chem. Soc.* **1965**, *87*, 685-692.

(b) Dewar, M. J. S.; Gleicher, G. J. *J. Am. Chem. Soc.* **1965**, *87*, 692-696.

(c) Dewar, M. J. S.; de Llano, C. *J. Am. Chem. Soc.* **1969**, *91*, 789-795.

(d) Dewar, M. J. S.; Morita, T. *J. Am. Chem. Soc.* **1969**, *91*, 796-802.

(e) Dewar, M. J. S.; Morita, T. *J. Am. Chem. Soc.* **1969**, *91*, 802-806.

[91] Hess, B. A.; Shaad, L. J. *J. Am. Chem. Soc.* **1971**, *93*, 305-310.

[92] Zhou, Z.-X. *Int. Rev. Phys. Chem.* **1992**, *11*, 243-261.

[93] Jug, K.; Köster, A. M. *J. Phys. Org. Chem.* **1991**, *4*, 163-169.

[94] Katritzky, A. R.; Barczynski, P.; Musumarra, G.; Pisano, D.; Szafran, M. *J. Am. Chem. Soc.* **1989**, *111*, 7-15.

[95] Malaspina, L.; Bardi, G.; Gigi, R. *J. Chem. Thermodyn.* **1974**, *6*, 1053-1064.

[96] Stull, D. R.; Westrum, Jr., E. F.; Sinke, G. C. *"The Chemical Thermodynamics of Organic Compounds"* Wiley, New York, N. Y., **1969**.

[97] Taylor, R.; Walton, R. M. *Nature* **1993**, *363*, 685-693.

[98] (a) Fagan, P. J.; Calabrese, J. C.; Malone, B. *Acc. Chem. Res.* **1992**, *25*, 134-142.

(b) Fagan, P. J.; Calabrese, J. C.; Malone, B. *Science* **1991**, *252*, 1160-1161.

[99] Balch, A. L.; Catalano, V. J.; Lee, J. W.; Olmstead, M. M.; Parkin, S. R. *J. Am. Chem. Soc.* **1991**, *113*, 8953-8955.

[100] Roth, G.; Adelmann, P. *J. Phys. I (France)* **1992**, *2*, 1541-1548.

[101] (a) Hawkins, J. M. *Acc. Chem, Res.* **1992**, *25*, 150-156.

(b) Hawkins, J. M.; Meyer, A.; Lewis, T. A.; Loren, S.; Hollander, F. J. *Science* **1991**, *252*, 312-313.

[102] Hedberg, K.; Hedberg, L.; Bethune, D. S.; Brown, C. A.; Dorn, H. C.; Johnson, R. D.; de Vries, M. *Science* **1991**, *254*, 410-412.

[103] Wudl, F. *Acc. Chem, Res.* **1992**, *25*, 157-161.

[104] Saunders, M.; Jiménez-Vázquez, H. A.; James Cross, R.; Mroczkowski, S.; Freedberg, D. I.; Anet, F. A. L. *Nature* **1994**, *367*, 256-258.

[105] Trost, B. M.; Bright, G, M.; Frihart, C.; Brittelli, D. *J. Am. Chem. Soc.* **1971**, *93*, 737-744.

[106] Adams, G. B.; Sankey, O. F.; Page, J. B.; O'Keeffe, M.; Drabold, D. A. *Science* **1992**, *256*, 1792-1795.

[107] Man, N.; Nagano, Y.; Kiyobayashi, T.; Sakiyama, M. *J. Phys. Chem.* **1995**, *99*, 2254-2255.

[108] (a) Kroto, H. W. *Science* **1988**, *242*, 1139-1145.

(b) Kroto, H. W.; McKay, K. *Nature* **1988**, *331*, 328-331.

(c) Zhang, Q. L.; O'Brien, S. C.; Heath, J. R.; Liu, Y.; Curl, R. F.; Kroto, H. W.; Smalley, R. E. *J. Phys. Chem.* **1986**, *90*, 525-528.

[109] (a) Bennemann, K. H.; Reichardt, D.; Morán-López, J. L.; Kerner, R.; Penson, K. *Z. Phys.* **1994**, *D29*, 231-239.

(b) Morán-López, J. L.; Bennemann, K. H.; Cabrera-Trujillo, M, ; Dorantes-Dávila, J. *Solid State Commun.* **1994**, *89*, 977-981.

[110] Maiti, A.; Brabec, C. J.; Bernholc, J. *Phys. Rev. Lett.* **1993**, *70*, 3023-3026.

[111] (a) Iijima, S. *Nature* **1991**, *354*, 56-58.

(b) Hamada, N.; Sawada, S.; Oshiyama, A. *Phys. Rev. Lett.* **1992**, *68*, 1579-1581.

(c) Iijima, S.; Ajayan, P. M.; Ichihashi, T. *Phys. Rev. Lett.* **1992**, *69*, 3100-3103.

(d) Iijima, S.; Ichihashi, T.; Ando, Y. *Nature* **1992**, *356*, 776-778.

(e) Ebbson, T. W.; Ajayan, P. M.; Hiura, H.; Tanigaki, K. *Nature* **1994**, *367*, 519.

[112] (a) Ugarte, D. *Nature* **1992**, *359*, 707-709.

(b) Ugarte, D. *Europhys. Lett.* **1993**, *22*, 45-.
(c) Ugarte, D. *Chem. Phys. Lett.* **1993**, *207*, 473-479.
(d) de Heer, W. A.; Ugarte, D. *Chem. Phys. Lett.* **1993**, *207*, 480-485.
(e) Ugarte, D. *Carbon* **1994**, *32*, 1245-1248.
(f) Ugarte, D. *Carbon* **1995**, *33*, 989-993.

[113] Harris, P. J. F.; Tsang, S.-C.; Claridge, J. B.; Green, M. L. H. *J. Chem. Soc., Faraday Trans.* **1994**, *90*, 2799-2802.

[114] Yamada, K.; Kunishige, H.; Sawaoka, A. B. *Naturwissenschaften* **1991**, *78*, 450-452.

[115] Hatta, N.; Murata, K. *Chem. Phys. Lett.* **1994**, *217*, 398-402.

[116] Weathers, M. S.; Basset, W. A. *Phys. Chem. Minerals* **1987**, *15*, 105-112.

[117] (a) Kuznetsov, V. L.; Chuvilin, A. L.; Butenko, Yu. V.; Mal'kov, I. Yu.; Titov, V. M. *Chem. Phys. Lett.* **1994**, *222*, 343-348.
(b) Kuznetsov, V. L.; Mal'kov, I. Yu.; Chuvilin, A. L.; Moroz, E. M.; Kolomiichuk, V. N.; Shaichutdinov, Sh. K.; Butenko, Yu. V. *Carbon* **1994**, *32*, 873-882.
(c) Mal'kov, I. Yu.; Titov, V. M.; Kuznetsov, V. L.; Chuvilin, A. L. *Fiz. Gorenia i Vzryva* **1994**, *30*, 130-132.

[118] Tománek, D.; Zhong, W.; Krastev, E. *Phys. Rev.* **1993**, *B48*, 15461-15464.

[119] Hess, Jr., B. A.; Schaad, L. J. *J. Org. Chem.* **1986**, 3902-3903.

[120] (a) Klein, D. J.; Seitz, W. A.; Schmalz, T. G. *Nature* **1986**, *323*, 703-706.
(b) Schmalz, T. G.; Seitz, W. A.; Klein, D. J.; Hite, G. E. *Chem. Phys. Lett.* **1986**, *130*, 203-207.

[121] Hosoya, H. *Comput. Math. Appls.* **1986**, *B12*, 271-.

[122] Charlier, J.-C.; Michenaud, J.-P. *Phys. Rev. Lett.* **1993**, *70*, 1858-1861.

[123] Dunlap, B. I. *Phys. Rev.* **1992**, *B46*, 1933-1936.

[124] (a) Itoh, S.; Ihara, S.; Kitakami, J. *Phys. Rev.* **1993**, *B47*, 1703-1704.
(b) Ihara, S.; Itoh, S.; Kitakami, J. *Phys. Rev.* **1993**, *B47*, 12908-12911.
(c) Ihara, S.; Itoh, S.; Kitakami, J. *Phys. Rev.* **1993**, *B48*, 5643-5647.
(d) Itoh, S.; Ihara, S. *Phys. Rev.* **1993**, *B48*, 8323-8328.
(e) Itoh, S.; Ihara, S. *Phys. Rev.* **1993**, *B49*, 13970-13974.

[125] Mackay, A. L.; Terrones, H. *Nature* **1991**, *352*, 762.

[126] (a) Lenosky, T. J.; Gonze, X.; Teter, M.; Elser, V. *Nature* **1992**, *355*, 333-335.
(b) Townsend, S. J.; Lenosky, T. J.; Muller, D. A.; Nichols, C. S.; Elser, V. *Phys. Rev. Lett.* **1992**, *69*, 921-924.

[127] Vanderbilt, D.; Tersoff, J. *Phys. Rev. Lett.* **1992**, *68*, 511-513.